1991

A.J. Baddeley, R.A. Moyeed, C.V. Howard, A. Boyde

Analysis of a three-dimensional point pattern with replication

Department of Operations Research, Statistics, and System Theory Report BS-R9124 September

CWI, nationaal instituut voor onderzoek op het gebied van wiskunde en informatica

CWI is the research institute of the Stichting Mathematisch Centrum, which was founded on February 11, 1946, as a non-profit institution aiming at the promotion of mathematics, computer science, and their applications. It is sponsored by the Dutch Government through the Netherlands organization for scientific research (NWO).

Analysis of a Three-Dimensional Point Pattern with Replication

A. J. Baddeley
R. A. Moyeed[1]
C. V. Howard[2]
A. Boyde[3]

CWI
P.O. Box 4079, 1009 AB Amsterdam
The Netherlands

[1] *School of Mathematical Sciences, University of Bath*
Claverton Down, Bath BA2 7AY, UK

[2] *Quantitative 3-D Microscopy Research Group*
Department of Human Anatomy and Cell Biology
University of Liverpool
P.O. Box 147, Liverpool L69 3BX, UK

[3] *Department of Anatomy and Embryology,*
University College London, London WC1E 6BT, UK

Techniques for analysing three-dimensional spatial point patterns are demonstrated on data from a confocal microscope recording the locations of cells in 3D. New computational techniques are proposed for edge corrections and empty space measurement. A novel feature of the data is replication and nesting in a sampling design: multiple spatial patterns were observed from each of several animals. For this we develop a ratio regression approach.

AMS Mathematics Subject Classification (1991 Revision): 62H11, 62M30, 60D05.
Key Words & Phrases: Confocal microscopy, distance transform, empty space function, K function, Monte Carlo inference, osteocyte lacunae, replicated spatial patterns, spatial statistics, tandem scanning reflected light microscope, three dimensional imaging.
Note: This paper has been submitted for publication.

Report BS-R9124
ISSN 0924-0659
CWI
P.O. Box 4079, 1009 AB Amsterdam, The Netherlands

Introduction

The three-dimensional structure of living tissue and solid materials can now be observed directly by imaging techniques such as confocal microscopy (Wilson, 1990). Existing statistical methods for analysing 'spatial' point patterns (Ripley, 1981, 1988; Diggle, 1983) are mostly 2 dimensional; although the general theory works in d dimensions, there are problems for $d > 2$ with the complexity of edge correction, increased bias and variance due to edge effects, and extra computational load.

At the same time, the increased ability to capture and store data and to navigate through the three-dimensional material has made it possible to collect *replicated* samples of a spatial pattern, for example, 3-dimensional images of several different locations in the material. Replication was not studied in the earlier statistical theory; indeed its absence caused difficulties.

This paper is a worked example of the analysis of a three-dimensional spatial pattern with replication. Our data are three-dimensional coordinates giving the positions of osteocyte lacunae in the skull bones of Macaque monkeys observed using a tandem-scanning reflected light microscope at University College London (Howard et al, 1985; Baddeley et al, 1987). Osteocyte lacunae are holes in solid bone, occupied by bone cells in life. Several sampling volumes (called 'bricks') were taken within each animal skull, sufficiently far apart to assume independence, and the positions of the lacunae within each brick were recorded. The main scientific questions concerned (a) the density of lacunae per unit volume, and whether this density is uniform; (b) spatial pattern in the arrangement of neighbouring lacunae; (c) variability in lacunar density and spatial pattern within and between animals.

The three-dimensional version of the standard K statistic was described in Baddeley et al (1987). Braendgaard and Gundersen (1986) and Bjaalie and Diggle (1990) have analysed 2D projections of 3D patterns, obtained from physical sections. Recently Diggle et al (1991) and König et al. (1991) have described three-dimensional versions of the F, G and K statistics. In the present paper we focus on statistical properties of these estimators.

Replicated data from a confocal microscope were first collected by Howard et al (1985) and a ratio regression approach was developed in Baddeley et al (1987). König et al (1991) found huge variations in estimates of point density λ between replicated 3D samples, and concluded that their data (three replicates per animal) were insufficient to support quantitative conclusions. Diggle et al (1991) have developed a bootstrap approach to inference for replicated spatial patterns. Here we shall extend the simpler ratio regression approach to F and G as well as K.

A special feature of many three-dimensional spatial data sets is a distinguished direction, the "z-axis", representing e.g. height or distance from the viewing device. Point patterns may often be regarded as uniform in the other two "horizontal" directions but not in the z direction; or they may have a different error structure in the z direction. In our data, the z coordinate represents depth inside the skull bone, and has a definite reference origin (the bone surface) as well as direction; the x and y coordinates are not so strongly distinguished. This makes the analysis of such data halfway between genuine 3D points and marked 2D points. The standard assumption of stationarity and isotropy may not be valid here.

The data are described in the next section. Section 2 gives some theoretical background and numerical methods. Sections 3 and 4 develop an approach to the replication and nested sampling design. Section 5 records our analysis of the data.

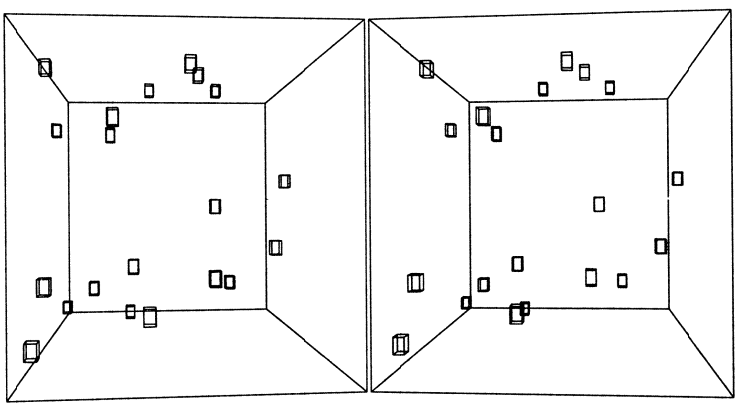

Figure 1: Stereo-pair of the data in a sampling brick 82 × 100 microns wide and 60 microns deep, showing each point as a 3 micron cube.

1 Data

The experimental technique and sampling protocol are described by Howard et al (1985) and Baddeley et al (1987). We examined three intact adult skulls and one calvarium (incomplete skull), all attributed to the Macaque monkey *Macaca fascicularis*, from the collection of University College London. The focal plane of the confocal microscope was initially positioned 10μm below the cranial surface, then racked down through the bone until no further lacunae could be visualised. The depth z of the centre of each lacuna was determined by adjusting the fine focus racking control to yield maximum brightness. The (x, y, z) coordinates of the centre of each lacuna were recorded only if (x, y) lay within a graduated rectangular frame fixed to the screen. The 3-dimensional sampling volume was therefore a rectangular box, of dimensions $82 \times 100 \times d$ microns, called a "brick". The depth d varied from brick to brick.

Ten bricks per animal were examined, arranged approximately in a rectangular grid pattern, with at least one brick width separating each pair of bricks. The initial brick position was determined randomly by applying a randomly-generated coordinate shift to the moving stage. Subsequent bricks were reached using the coarse controls of the microscope stage, in accordance with the grid pattern.

Figure 1 shows the pattern from brick 10 of animal 4 displayed as a binocular stereo view, which each point has been displayed as a cube of side 3 microns.

2 Theory

General theory of point processes can be consulted in Daley and Vere-Jones (1989); for statistical methods see Ripley (1981, 1988), Diggle (1983), Stoyan et al (1987) and Cox and Isham (1980). In the standard nonparametric approach (Ripley, 1981), simple summary statistics of the pattern are interpreted as unbiased estimates of the corresponding quantities for the point process, under minimal assumptions of stationarity. Popular summary statistics for a two-dimensional point pattern are the functions $\hat{K}, \hat{G}$ and $\hat{F}$, which are edge-corrected versions of the empirical distributions of (respectively) the distances between all pairs of points in the pattern, the distance from each point in the pattern to its nearest neighbour in the pattern, and the distance from a randomly chosen point in the sampling window to the nearest point of the pattern. We shall adapt each of these functions to 3 dimensions (see also Diggle et al., 1991 and König et al, 1991).

Estimation is plagued by *edge effects* resulting from the inability to search outside the sampling window; Miles (1974), Ripley (1988, chap. 3) and Stoyan et al. (1987, §4.6) give illuminating general discussions. Edge effects are worse in higher dimensions: for example, in a three-dimensional unit cube, the points that are closer than 0.1 units away from the boundary occupy about half the volume. If an unbiased estimate of a parameter is required (e.g. for comparative purposes) there is no alternative but to seek bias corrections, which sometimes involve throwing away data. Corrections for edge effects in K, G and F for two dimensions were given by Ripley (1981, 1988) and Hanisch (1984); some of these corrections have been adapted to 3D by Baddeley et al (1987), Diggle et al (1991) and König et al (1991). In the present approach, we are further able to exploit the replication to develop efficient unbiased estimators and associated variance estimates.

Edge effects can largely be ignored in hypothesis testing. In the standard Monte Carlo test of a simple null hypothesis, one uses an uncorrected (hence biased) version of a summary statistic, simulates 99 realizations of the null hypothesis and ranks the 100 results according to some one-dimensional criterion. See Ripley (1981), Diggle & Gratton (1984), Hall (1988), Ripley (1988), Diggle et al (1991) and König et al (1991).

2.1 Assumptions

The point pattern observed inside a sampling region B is taken to be a realization of a spatial point process $\mathbf{N}(\cdot)$. For estimation purposes one may want to assume the process is 'stationary' (invariant under translations of $\mathbb{R}^3$) and 'isotropic' (invariant under rotations) as regards moments of order up to k ("k-th order stationarity") or all probability distributions associated with the process ("a.s. stationarity"). These are the minimum assumptions in order that the position and orientation of sampling regions need not be recorded, and that replicated data may be pooled. Usually we will only assume 'horizontal stationarity', i.e. invariance under rotations and translations of the (x, y) plane, and will test for full invariance.

The usual null hypothesis (and benchmark for estimation purposes) is that $\mathbf{N}(\cdot)$ is a uniform Poisson process with unspecified rate $\lambda > 0$ (e.g. Ripley, 1981). The Poisson process serves as the model of complete spatial randomness; departures from Poisson (within the class of a.s. stationary and isotropic processes) are interpreted as indications of 'pattern'. These are traditionally lumped into (a) 'clustered' and (b) 'repulsive' or 'ordered' alternatives (Diggle, 1983).

For departures from stationarity and isotropy, the natural asymmetry with respect to z suggests a class of alternative hypotheses such as the nonuniform Poisson process with rate $\lambda(z)$ depending on z, and Gibbs processes with anisotropic interaction potentials (Stoyan et al, 1987).

2.2 Intensity

First consider the average density of random points per unit volume. Let $\mathbf{N}(B)$ be the number of random points falling in a region $B \subset \mathbb{R}^3$. If $\mathbf{N}(\cdot)$ is first order stationary then

$$\mathbb{E}\mathbf{N}(B) = \lambda \, \mathbf{vol}(B)$$

for a constant λ independent of B called the intensity. Thus an unbiased estimator of λ is simply the observed density

$$\widehat{\lambda} = \frac{\mathbf{N}(B)}{\mathbf{vol}(B)} \tag{1}$$

for any window B. If $\mathbf{N}(\cdot)$ is an arbitrary process then

$$\Lambda(B) = \mathbb{E}\mathbf{N}(B)$$

defines its intensity *measure* Λ. Under mild conditions Λ can be represented as the integral of a rate function $\lambda(x, y, z)$. A particularly interesting alternative to stationarity $\lambda(x, y, z) = \lambda > 0$ is "horizontal stationarity" $\lambda(x, y, z) = \lambda_1(z) \geq 0$. To test the null hypothesis of a stationary Poisson process of unspecified intensity λ against the alternative of a horizontally stationary *Poisson* process with unspecified intensity $\lambda_1(z)$, we note that the z coordinates of the points in a rectangular box or prism B form a one-dimensional inhomogeneous Poisson process. Conditional on the number of points, the z coordinates are i.i.d. with probability density proportional to $\lambda_1(\cdot)$, and we can apply standard nonparametric tests for the uniform distribution.

2.3 Empty space function F

Now consider summary statistics for the spatial pattern assuming stationarity and isotropy. The 'empty-space function' F of a point process (a.s. stationary and isotropic) is the probability distribution of the distance from an arbitrary point (say 0) to the nearest random point:

$$F(r) = \mathbb{P}\mathbf{r}\{\mathbf{N}(S(0, r)) > 0\}$$

where $S(x,r)$ is the sphere of radius r around point x in $\mathbb{R}^3$ (Ripley, 1981, 1988; Diggle,1983). Note $p(r) = 1 - F(r)$ equals the expected fraction of volume in $\mathbb{R}^3$ occupied by points x which are at least r units distant from the nearest random point of the process $\mathbf{N}(\cdot)$. For a uniform Poisson process of intensity λ,

$$F(r) = 1 - \exp\{-4/3 \lambda \pi r^3\}. \tag{2}$$

Values of $F(r)$ greater than the Poisson value suggest there is repulsion or ordering in the point pattern; lower values suggest attraction or clustering.

Typically F is estimated by taking a fine grid in the sampling region B and computing the distance from each grid point to the nearest observed point of the process. However edge effects arise because we are unable to search for points outside B. The only unbiased estimator of F currently in use is the *minus-sampling* estimator

$$\begin{aligned} \widehat{F}_-(r) &= \frac{\mathbf{vol}\left(B_{(-r)} \cap \left(\bigcup_j S(X_j, r)\right)\right)}{\mathbf{vol}\left(B_{(-r)}\right)} \\ &= \frac{\mathbf{vol}\{x \in B_{(-r)} : \min_k ||x - X_k|| \leq r\}}{\mathbf{vol}\left(B_{(-r)}\right)} \end{aligned} \tag{3}$$

where $X_k : k = 1, \ldots, \mathbf{N}(B)$ are the observed points, and

$$B_{(-r)} = \{x \in B : S(x,r) \subset B\} \tag{4}$$

is the set of points of B more than r units distant from the boundary of B. That is, in estimating $F(r)$ one ignores points x that are closer than r units from the boundary of B; the points x 'counted' in the numerator of (3) are those for which it is known that the closest point is within a distance r. This estimator is clearly unbiased pointwise for F. Minus sampling was first discussed by Miles (1974) for planar problems.

The two-dimensional analogue of (3) is typically computed by evaluating for each point x in a fine rectangular grid, the distance to the nearest point:

$$d(x) = \min_k ||x - X_k||$$

and counting the grid points x in $B_{(-r)}$ for which $d(x) \leq r$. Diggle and Matérn (1981) discuss optimal choice of the grid, and Lotwick (1981) describes an algorithm (based on the Dirichlet tessellation) for computing the areas exactly. However, a good approximation to $d(x)$ can be computed very rapidly for all x on a fine rectangular grid using the *distance transform* algorithm developed in image processing (Rosenfeld and Pfalz, 1968). This also works in higher dimensions (Borgefors, 1984, 1986). For accurate comparisons the expression $(4/3)\pi r^3$ in (2) should then be replaced by the digital volume of the sphere of radius r in this discrete approximation.

Minus sampling throws away part of the data; Diggle (1983) and others prefer to ignore edge effects and use the empirical distribution $\widehat{F}_B$ of the observed distances $d(x)$. Clearly $\widehat{F}_B$ is biased for F, but can be used in a Monte Carlo significance test of any simple hypothesis. This approach is appealing because it makes 'full use' of the data, but with replicated data we cannot pool $\widehat{F}_B$ from different bricks B since the bias and variance of $\widehat{F}_B(r)$ depend on the geometry of B. For the Poisson process

$$\mathbb{E}\widehat{F}_B(r) = \frac{1}{\mathbf{vol}(B)} \int_B \left\{1 - e^{-\lambda \mathbf{vol}(B \cap S(x,r))}\right\} dx, \tag{5}$$

while if we condition on the number of points n then $1 - \exp(-u)$ should be replaced by $1 - (1-u)^n$. An analytic expression for the integrand is given in the Appendix.

2.4 Estimation of G

The function G is the distribution of the distance from *a typical point of the process* to the nearest other point: loosely

$$G(r) = \mathbb{P}\mathbf{r}\{\mathbf{N}(S(x,r)) > 1 | \text{ point at } x\}$$

where x is arbitrary. This can be defined for an a.s. stationary process by

$$G(r) = \frac{1}{\lambda \mathbf{vol}(B)} \mathbb{E} \sum_{X_k \in B} 1\{\mathbf{N}(S(X_k, r)) > 1\} \tag{6}$$

where B is arbitrary. For a Poisson process $G(r) = 1 - \exp\{-(4/3)\lambda\pi r^3\}$; again, this is taken as a benchmark for interpretation of empirical G-functions. Edge effects arise because we can only observe nearest neighbour distances within B,

$$s_k = \min_{X_\ell \in B, \ell \neq k} ||X_k - X_\ell||, \quad X_k \in B.$$

Ripley (1981, see Ripley, 1988, chap. 3) introduced the minus sampling estimator

$$\widehat{G}_1(r) = \frac{\sum_j 1\{s_j \leq r\} 1\{x_j \in B_{(-r)}\}}{\sum_j 1\{x_j \in B_{(-r)}\}}; \tag{7}$$

the denominator is the number of all points lying more than r units from the boundary of B, and the numerator is the number of these that have $s_j \leq r$.

Hanisch (1984; see Stoyan et al, 1987, p. 128, Ripley, 1988, chap. 3) observed that in general $\widehat{G}_1$ will not be an increasing function, and may have values greater than 1. Hanisch developed two further edge-corrected estimators of G, of which we shall use

$$\widehat{G}_3(r) = \frac{\sum_j 1\{s_j \leq r\} 1\{x_j \in B_{(-s_j)}\}}{\sum_j 1\{x_j \in B_{(-s_j)}\}}. \tag{8}$$

This consists in restricting both numerator and denominator of (7) to points X_k for which s_k is known to be the 'true' nearest neighbour distance, i.e. for which the nearest other point is closer than the boundary. Clearly $\widehat{G}_3$ is a distribution function; Hanisch (1984) showed it is pointwise consistent in the limit as the sampling region expands to cover $\mathbb{R}^3$.

Edge effects can be severe for G, so it becomes appealing to employ the uncorrected empirical distribution $\widehat{G}_B$ of the observed s_k. This can be treated in the same way as $\widehat{F}_B$. For the Poisson process $\mathbb{E}\widehat{G}_B(r) = \mathbb{E}\widehat{F}_B(r)$ as given by (5); but if we condition on the number n of points, then $\exp(-x)$ in (5) is replaced by $(1-x)^{n-1}$.

2.5 Estimation of K

Finally $K(r)$ is the mean number of other points of the process that lie within a radius r of a typical point of the process, divided by the intensity λ:

$$K(r) = \frac{\mathbb{E}\{\mathbf{N}(S(x,r)) - 1 | \text{ point at } x\}}{\lambda}.$$

This can be defined whenever the process is merely *second order* stationary, as

$$\lambda K(r) = \frac{1}{\lambda \mathbf{vol}(B)} \mathbb{E} \sum_{X_k \in B} \sum_{X_\ell \neq X_k} 1\{||X_k - X_\ell|| \leq r\} \tag{9}$$

(where X_ℓ is not restricted to lie inside B). If the process is also second order isotropic, then $K(r)$ completely determines the second order moments of the process. For a Poisson process

$$K(r) = \frac{4}{3}\pi r^3$$

and again this serves as a benchmark for the interpretation of empirical K-functions.

Ripley (1988, pp. 31–35; see Stoyan et al, 1987, pp. 122-126) describes several edge effect corrections for estimating K in two dimensions. Here we consider 3 dimensional versions of the 'border', 'translation' and 'isotropic' corrections. The 'border' correction estimate is

$$\widehat{K}_b(r) = \frac{\mathbf{vol}\left(B_{(-r)}\right)}{\mathbf{N}\left(B_{(-r)}\right)^2} \sum_{X_k \in B_{(-r)}} \sum_{X_\ell \in B} 1\{0 < ||X_k - X_\ell|| \le r\}; \tag{10}$$

this is a straight application of minus sampling to (9), and is valid for any second-order stationary process. The sum is an unbiased consistent estimator of $\lambda^2 \mathbf{vol}\left(B_{(-r)}\right) K(r)$ so (10) is consistent and approximately unbiased.

The (Miles-Lantuéjoul) 'translation corrected' estimate is

$$\widehat{K}_t(r) = \frac{\mathbf{vol}\,(B)^2}{\mathbf{N}\,(B)^2} \sum_{X_k \in B} \sum_{X_\ell \neq X_k} \frac{1\{||X_k - X_\ell|| \le r\}}{\gamma_B(X_k - X_\ell)} \tag{11}$$

where γ_B is the 'set covariance'

$$\gamma_B(v) = \mathrm{vol}\{x \in B : x + v \in B\}.$$

Again this is valid for any second-order stationary process. If additionally the process is known to be isotropic, then the 'isotropic correction' estimate

$$\widehat{K}_i(r) = \frac{\mathbf{vol}\,(B)}{\mathbf{N}\,(B)^2} \sum_{X_k \in B} \sum_{X_\ell \neq X_k} \frac{1\{||X_k - X_\ell|| \le r\}}{w_B(X_k, X_\ell) s_B(||X_k - X_\ell||)} \tag{12}$$

is valid, where $w_B(X_k, X_\ell)$ is an edge correction equal to the proportion of the surface area of the sphere with centre at X_k and radius $||X_k - X_\ell||$ which lies within the sampling window B:

$$w_B(x, y) = \frac{\mathbf{area}(\partial S(x, ||x - y||) \cap B)}{\mathbf{area}(\partial S(x, ||x - y||))}$$

where $\partial S(x, r)$ is the surface of the sphere $S(x, r)$. Meanwhile $s_B(r)$ is a global geometry correction

$$s_B(r) = \frac{\mathrm{vol}\{x \in B : ||x - y|| = r, \text{ some } y \in B\}}{\mathbf{vol}\,(B)} = \frac{\mathrm{vol}\{x \in B : R(x, r) \cap B \neq \emptyset\}}{\mathbf{vol}\,(B)};$$

it was first noted by Hanisch (1984) that the term $s_B(r)$ is needed for larger r. We give analytic expressions for w_B, s_B in the Appendix for the case of a rectangular box.

The sum in (12) is a consistent unbiased estimator of

$$Y(r) = \lambda^2 \mathbf{vol}\,(B)\, K(r)$$

(in the limit as the sampling region expands to cover $\mathbb{R}^3$); hence (12) is consistent and approximately unbiased.

In two dimensions, Ripley (1981) and Diggle (1983, p. 71) generally recommend that estimates of $K(r)$ should only be employed for r less than half the minimum side length of the sampling rectangle. However, we will be able to go to larger values of r by pooling information from replicates.

2.6 Comments

The functions F, G and K should not be read as *characterisations* of the point process. For example, two quite different processes may have the same K function (Baddeley & Silverman, 1984). This insensitivity is a feature of most current techniques in spatial statistics. Analysis of a point pattern should normally include several measures of interaction.

Alternatives to F, G, K may be proposed if there is a suggestion of anisotropy or directional asymmetry in the pattern. The sphere $S(x,r)$ used in the definitions of F, G, K may be replaced by a cylinder or ellipsoid, so that the statistic becomes a function of 2 or 9 parameters respectively. This is equivalent to replacing ordinary Euclidean distance $||a-b||$ by some other metric. The edge corrections discussed here continue to hold, except for the isotropic correction for K. The simplest way to induce an 'isotropic' correction for the ellipsoidal K-function is to subject the point pattern data to a linear transformation which maps the ellipse to a sphere, then apply the isotropic estimator. Note that a linear transformation maps a Poisson process to a Poisson process, but e.g. a hard core process (Stoyan et al, 1987) is mapped to a process with genuinely isotropic pattern.

3 Ratio estimation

It does not seem to have been pointed out in the spatial statistics literature that the usual statistics $\widehat{K}, \widehat{G}, \widehat{F}$ are ratio estimators. Equations (1), (3), (7), (8), (10), (11), (12) define statistics T of the form $T = U/V$ where

$$t = \frac{\mathbb{E}U}{\mathbb{E}V}$$

is the parameter of interest. In all but (1) and (3) the denominator V is not fixed and T is typically biased for t, though approximately unbiased and consistent (asymptotically in the size of the sampling region). When replicated bivariate data (U_j, V_j) are available, it is then appropriate to use a ratio regression model as we discuss below.

3.1 Ratio regression

Consider the model (Cochran, 1977; Cruz Orive, 1980)

$$U_j = t\,V_j + e_j,\ j = 1, \ldots, m \tag{13}$$

where the errors e_j are conditionally independent given the V_j, with

$$\mathbf{Var}\,(e_j | V_j) \propto V_j^{\alpha} \tag{14}$$

for some $\alpha > 0$. The naive estimator of t is the sample mean of individual ratios $T_j = U_j/V_j$,

$$\tilde{t} = \frac{1}{m} \sum_{j=1}^{m} \frac{U_j}{V_j}$$

but this is biased and not consistent as the number of *replications* increases. If the V_i were fixed design points, the best linear unbiased estimator of the ratio parameter t would be

$$\widehat{t} = \frac{\sum_j V_j^{1-\alpha} U_j}{\sum_j V_j^{2-\alpha}}$$

i.e. the weighted average of the T_j with weights inversely proportional to variance. In case $\alpha = 2$ this is the sample average of the T_j, while if $\alpha = 1$ it is a ratio of averages

$$\widehat{t} = \frac{\sum U_j}{\sum V_j}. \tag{15}$$

The same approach can be used when the V_j are random variables (so that $\widehat{t}$ is unbiased but is BLUE only conditionally upon the V_j's).

The bias and variance of (15) are then (to first order using the delta method, see Cochran, 1977, pp. 161, 154)

$$\mathbb{E}\left\{\widehat{t} - t\right\} \approx \frac{t}{m}\left\{C_{uu} - C_{uv}\right\} \tag{16}$$

$$\mathbf{Var}\,(\widehat{t}) \approx \frac{t^2}{m}\left\{C_{uu} + C_{vv} - 2C_{uv}\right\} \tag{17}$$

where C_{uu}, C_{uv}, C_{vv} are the entries in the covariance matrix of $(\frac{U}{\mathbb{E}U}, \frac{V}{\mathbb{E}V})$. Note that the bias and variance both decrease as m^{-1} whereas the sample mean of the T_j's has constant nonzero bias.

Substituting the sample values $\widehat{t}, C_{uu}, C_{uv}, C_{vv}$ in (17) yields an empirical estimate of the variance of (15). The goodness of fit to the ratio regression model (13–14) can be adjudged from a scatter plot, residual plot or from a formal significance test assuming the e_j's are independent normal errors.

Improved estimators of t are available when $\mathbb{E}V$ is known (e.g. the Hartley-Ross estimator, Cochran, 1977, p. 174) or in sufficiently large samples using the jackknife (Durbin, 1959) but we doubt their applicability to the present data.

3.2 Application to F,G,K

We will now argue that the model (13)-(14) may be applied to the estimation of λ, $K(r)$, $G(r)$ and $F(r)$, with $\alpha = 1$. This will imply that e.g. the best estimate of $F(r)$ is the ratio of total numerator to total denominator in (3),

$$\widehat{F}_{ratio}(r) = \frac{\sum_{j=1}^{m} F^{(j)}(r)\mathbf{vol}\left(B_{j(-r)}\right)}{\sum_{j=1}^{m} \mathbf{vol}\left(B_{j(-r)}\right)} \tag{18}$$

where $F^{(j)}(r)$ is the estimate from data in B_j; and an estimate of the variance of this estimator may be obtained from (17).

The estimator (1) of λ is of the form $\widehat{\lambda} = U/V$ where $U = \mathbf{N}(B)$ = number of random points in B, $V = \mathbf{vol}(B)$. In a Poisson point process $\mathbf{Var}(\mathbf{N}(B)) = \mathbb{E}\mathbf{N}(B) = \lambda\mathbf{vol}(B)$ so (13)-(14) would apply with $\alpha = 1$. For more general processes, if one can assume that the effective range of spatial dependence is small compared to the size of the sampling region, then central limit theorems are available (e.g. Baddeley, 1980; Jolivet, 1980) which yield (13)-(14).

For the estimation of $F(r)$ (for fixed r) via (3), central limit theorems for Poisson superpositions of random sets (see e.g. Hall, 1989) suggest that the variance of the numerator of (3) may be taken as approximately proportional to the denominator.

For $K(r)$, take U to be the double sum in each of (10), (11), (12). Then Ripley (1981, 1988) and Hanisch (see Stoyan et al, 1987) have shown that $\mathbb{E}U/\mathbb{E}V = K(r)$ for any second order stationary and isotropic process. Ripley (1979) pointed out that U_j is a U-statistic

$$U_j = \sum_{k \neq \ell} u_j(X_{jk}, X_{j\ell})$$

where the summation is over all ordered pairs of distinct points in pattern $\mathcal{P}_j$, and function u_j depends on the geometry of B_j. Symmetrise u_j if necessary. For a uniform Poisson process, since V_j is a 1-1 function of $N = \mathbf{N}(B_j)$,

$$\begin{aligned} \mathbf{Var}(U_j|V_j) &= \mathbf{Var}(U_j|\mathbf{N}(B_j)) \\ &= 2N(N-1)\mathbf{Var}(u_j(X_1, X_2)) + 2N(N-1)(N-2)\mathbf{Var}(\mathbb{E}\{u_j(X_1, X_2)|X_1\}) \end{aligned}$$

where X_1, X_2 are independent uniformly distributed points in B_j. If edge effects could be ignored and if the B_j were all *identical*, the conditional expectation in the second term would be constant and (14) would hold with $\alpha = 1$. Ripley (1979) showed that in two dimensions the first term indeed dominates, at least for r no greater than one quarter of the smallest edge length of the sampling rectangle. In our case one can assume (14) holds when r is "sufficiently small" and when the dependence of u_j on B_j can be neglected.

Finally for G, the numerator U and denominator V of (7) clearly satisfy $\mathbb{E}U/\mathbb{E}V = G(r)$, and Hanisch (1984) showed that the same holds for (8). An argument similar to that for K above justifies (14), again if we ignore edge effects.

4 Analysis of variance

The full experiment analysed here is a one-way, nested design yielding point patterns $\mathcal{P}_{ij}$ from bricks $j = 1, \ldots, m$ in animals $i = 1, \ldots, n$. In place of (13) we now have

$$U_{ij} = t_i V_{ij} + e_{ij} \tag{19}$$

where the t_i are independent random effects with mean t and variance τ^2, and the e_{ij} are conditionally independent given t_i, with

$$\mathbf{Var}\,(e_{ij}|V_{ij}, t_i) = w_i V_{ij}. \tag{20}$$

Here t is the parameter to be estimated, τ^2 is the between-animal variance (of the random effects t_i), and w_i are nuisance parameters controlling the within-animal variability. The simpler model where $w_i = w$ did not seem justified for our data.

Our approach is to first estimate t_i and $\sigma_i^2 = \mathbf{Var}\,(\widehat{t}_i|t_i)$ by the ratio regression method above, giving values $\widehat{t}_i, \widehat{\sigma}_i^2$. Then we compute a sequence of estimates $t^{(k)}, \tau^2_{(k)}$ of t, τ^2 for $k = 0, 1, 2, \ldots$ by setting $t^{(0)}, \tau^2_{(0)}$ to be the sample mean and variance of the $\widehat{t}_i$, and iterating

$$t^{(k+1)} = \frac{\sum \widehat{t}_i / \left(\tau^2_{(k)} + \widehat{\sigma}_i^2\right)}{\sum 1 / \left(\tau^2_{(k)} + \widehat{\sigma}_i^2\right)} \tag{21}$$

$$\tau^2_{(k+1)} = \left(\frac{\sum \left[(\widehat{t}_i - t^{(k)})^2 - \widehat{\sigma}_i^2\right] \left(\tau^2_{(k)} + \widehat{\sigma}_i^2\right)^{-1}}{\sum 1 / \left(\tau^2_{(k)} + \widehat{\sigma}_i^2\right)} \right)_+ \tag{22}$$

where $(x)_+ = \max\{x, 0\}$. Here (21) takes the BLUE of t given observations $\widehat{t}_i$ with known variances; and (22) forms an unbiased estimate of τ^2 given $\widehat{t}_i$ when t and σ_i^2 are known. Together (21), (22) are respectively the E-step and M-step of the EM-algorithm for t, τ^2 in the model where the σ_i^2 are known and $\widehat{t}_i$ are normal, i.e. regarding $s_i = t_i - t$ as missing observations.

This method will be adopted when there is adequate data from each animal (specifically, when one expects $\widehat{\sigma}_i^2$ to be close to σ_i^2). When data is scarce we will resort to pooling all data (X_{ij}, Y_{ij}) and performing a simple ratio regression; this is equivalent to fixing $t_i = t, \tau^2 = 0, w_i = w$.

Steps (21–22) are iterated until convergence to produce estimates $\widehat{t}$ and $\widehat{\tau}^2$. The variance of $\widehat{t}$ can be estimated by the sample version of

$$\mathbf{Var}\,(\widehat{t}) \approx 1 / \sum_{i=1}^{n} b_i \tag{23}$$

where $b_i = 1/(\tau^2 + \sigma_i^2)$. The contributions to (23) associated with between-animal and within-animal, between-brick variation can be estimated respectively by

$$v_{\text{between}} = \tau^2 \frac{\sum b_i^2}{\left(\sum b_i\right)^2}, \tag{24}$$

$$v_{\text{within}} = \frac{b_i^2 \sigma_i^2}{\left(\sum b_i\right)^2}. \tag{25}$$

5 Analysis of our data

5.1 Intensity

Figure 2 is a scatter plot of point count n_{ij} against brick depth d_{ij} (proportional to volume) labelled by animal index i. Since brick depth was determined by our ability to see through the material, it might have some association with the spatial pattern, and would usually not be ancillary. However this association was thought neither relevant nor severe, so we condition on the d_{ij} and regard $\mathcal{P}_{ij}$ for $j = 1, \ldots, 10$ as independent realizations of the same point process $\mathbf{N}^{(i)}(\cdot)$ in $\mathbb{R}^3$, observed inside predetermined windows B_{ij}. The four animals furnish distinct point processes $\mathbf{N}^{(i)}(\cdot)$.

The ratio regression model (13–14) with $\alpha = 1$ looks plausible across bricks within each animal, but the data for animal 1 appear to have a different slope from the rest.

Table 5.1 shows the individual estimates n_{ij}/v_{ij} of cell density from each brick, the pooled ratio estimate $\widehat{\lambda}_i$ for each animal i using (15), and the estimated standard deviation $\widehat{\sigma}_i$ of $\widehat{\lambda}_i$ using (17).

Table 1: Estimates of λ (number per 10^6 cubic microns)

Animal	**λ estimates**										$\widehat{\lambda}_i$	$\widehat{\sigma}_i$
1	35.7	22.6	24.7	24.7	20.3	16.5	20.8	28.5	22.2	19.8	22.6	1.4
2	30.2	41.2	37.0	38.4	37.0	27.2	49.4	37.0	30.4	35.0	35.6	1.9
3	61.7	47.1	32.9	39.5	32.9	53.5	34.6	32.9	44.1	23.6	37.8	3.9
4	37.0	32.3	29.2	28.2	38.2	35.8	40.1	32.9	33.4	41.1	34.8	1.3

Applying (21–22) to the tabulated data gives $\widehat{\lambda} = 32.3$ with estimated variance 9.1 (standard error 3.0). The within-animal and between-animal variance contributions were 1.1 and 8.0 respectively. The estimate of population between-animal variance τ^2 was 31.4 (standard deviation 5.6) and a notional within-animal variance per sampling brick is $10 \times 1.1 = 11 = 3.3^2$.

The data for animal 1 appeared to be self-consistent but in conflict with the (mutually consistent) data for animals 2 to 4. Given the small number of animals it was difficult to decide whether to regard animal 1 as an outlier. When we repeated the analysis without animal 1, the EM procedure led to a zero estimate for τ^2, and weighted mean $\widehat{\lambda} = 35.1$ with estimated variance 1.5 (standard error 1.2).

In the light of this, the bone material was re-examined. Animal 1 was only represented by a calvarium (skull cap); from animals 2, 3 and 4 we had complete, intact skulls. Anatomical differences were found on closer examination. The three intact skulls recurved strongly behind the parietal-occipital suture, whereas in animal 1 the skull continued backwards. It was concluded that animal 1 came from a different species, though anatomically not very different. In the subsequent analysis we handle animal 1 separately and pool only across animals 2, 3 and 4.

5.2 Uniformity in z coordinate

The empirical distribution functions of the depths of the points in each brick were compared with the uniform distribution using a standard two-sided Kolmogorov-Smirnov test. Of the 40 bricks in the four animals the null hypothesis was rejected at the 5% level only in the case of two bricks belonging to animals 2 and 4. Inspection of the plots showed no strong suggestion of nonuniformity.

5.3 K function

Initially the K function was estimated separately from each brick. Figure 3 shows a comparison of K estimates for one brick using the translation and isotropic corrections. There was generally very close agreement between the two methods on this data set.

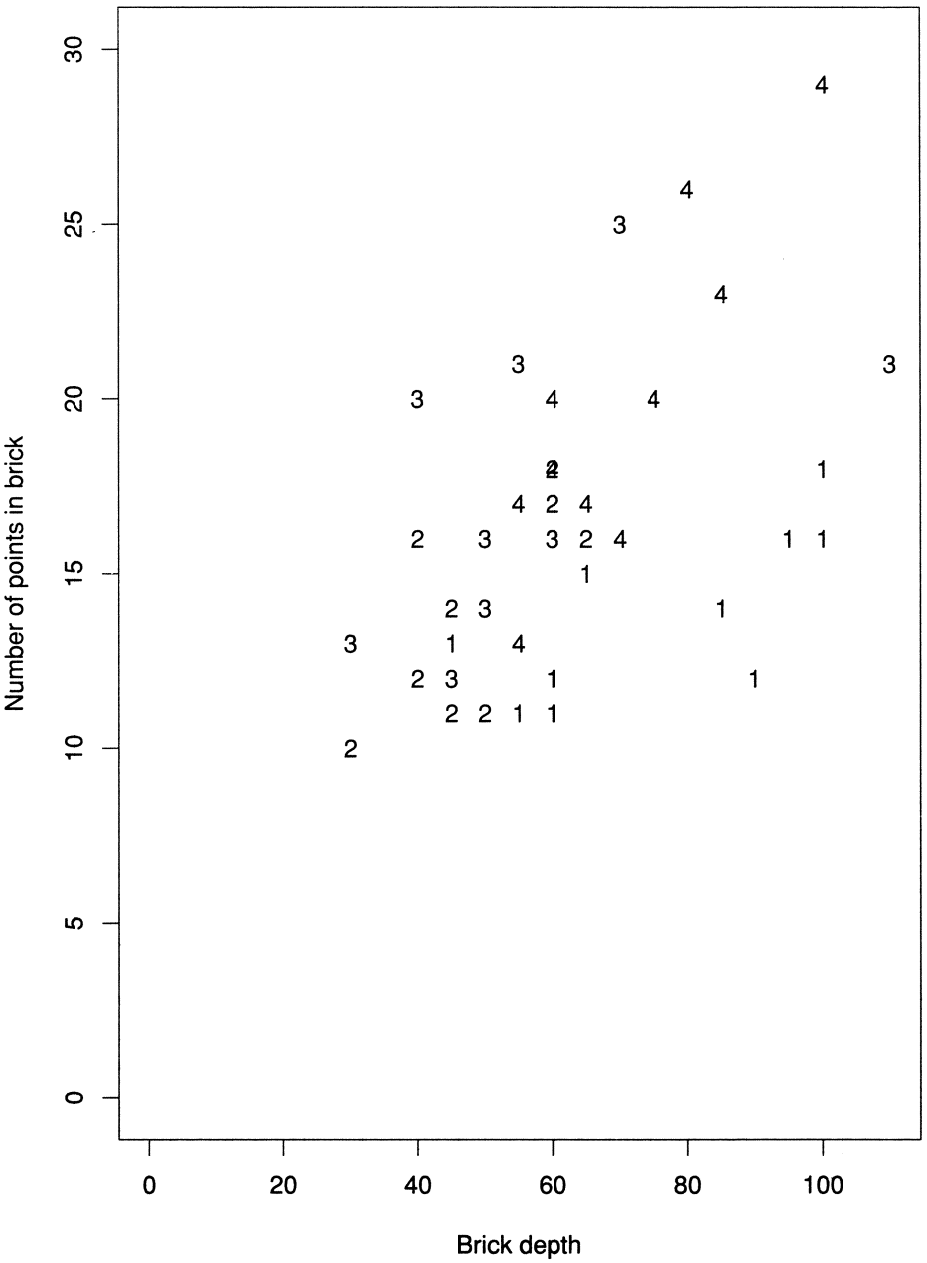

Figure 2: Scatterplot of cell count n_{ij} against brick depth d_{ij} labelled by animal index i.

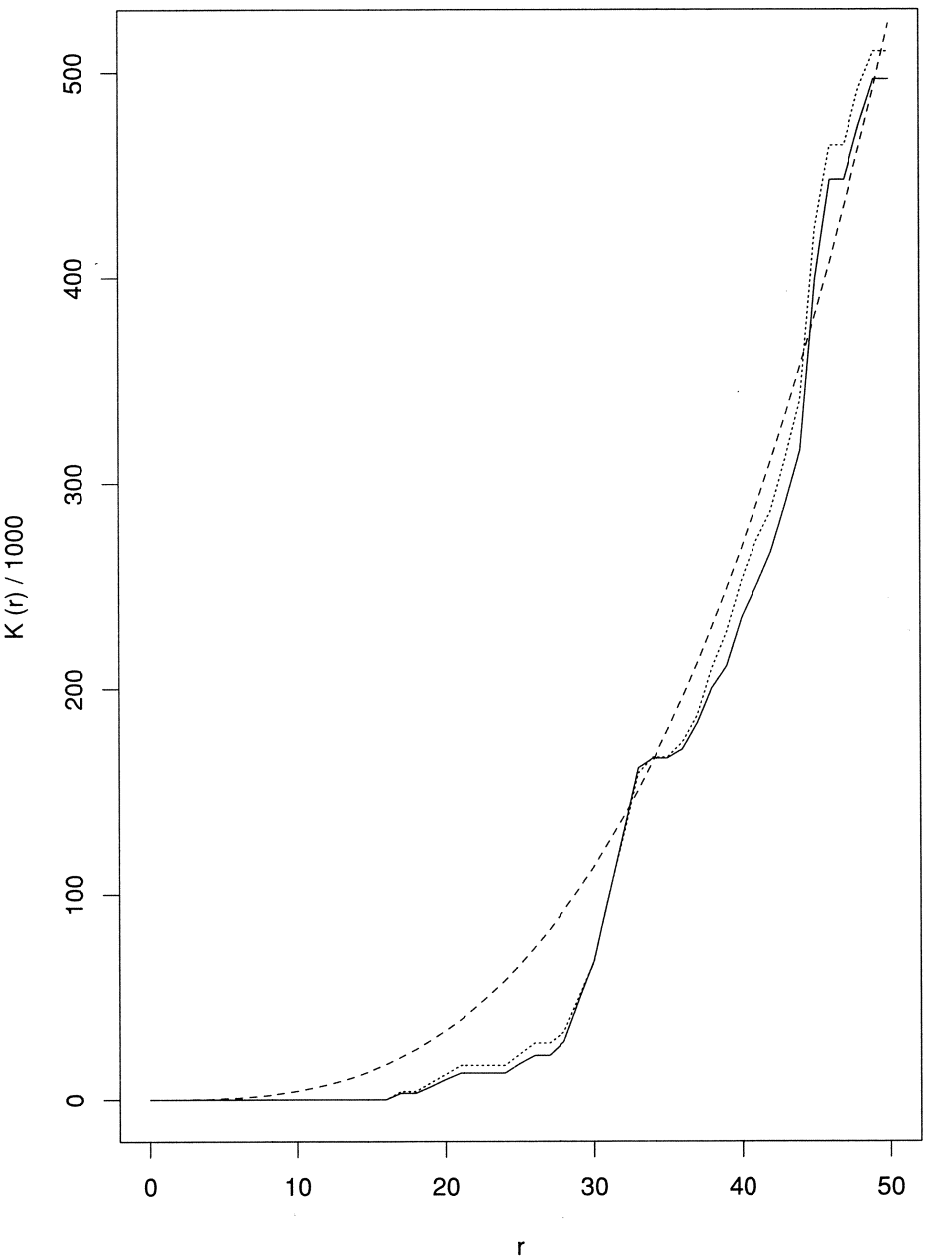

Figure 3: Comparison of estimates of K using Ripley-Hanisch isotropic correction (solid lines) and Miles-Lantuéjoul translation correction (dotted lines) for data from brick 1 of animal 4. Theoretical Poisson K function (broken lines) plotted for comparison.

Figure 4 shows for each animal the superimposed K estimates from all bricks. The theoretical K function for the Poisson process is plotted for comparison. There is a clear dip in the K function over the range 15 to 35 microns for all cases.

Ripley (1981) recommends plotting $\sqrt{K}(r)$ against r, because in two dimensions this transformation stabilises variance as well as linearising the plot. Diggle (1983) and others plot the 'residuals' $K(r) - \pi r^2$. In three dimensions $(\widehat{K})^{1/3}$ is linear but (contrary to König et al, 1991, p. 416) this does not stabilise variance. For three dimensional patterns we shall usually plot $K(r)$ against the theoretical Poisson curve $(4/3)\pi r^3$ in Q–Q style, Figure 5.

Figure 6 shows diagnostic scatter plots of the numerator and denominator of (11) for several choices of distance r, from all bricks and animals, with numerals identifying animals. The regression model looks broadly acceptable, although for small r many observations have $U = 0$, which might call for revision of the model. Note that, despite the differences previously encountered between animal 1 and the others, there seems to be general agreement in the K functions.

Figure 7 shows pooled K function estimates for each animal, using the ratio regression method to combine replicated bricks. The associated confidence bands are pointwise 95% confidence intervals computed from the estimated variances under the ratio regression method and the two-tailed 95% points of the t distribution with 9 degrees of freedom. These figures strengthen the interpretation of a strong dip in the range 15–35 microns. There is also good agreement between the K functions for the different animals.

Finally Figure 8 shows an overall K estimate formed by pooling all bricks in animals 2–4 using the E-M approach of section 4, with pointwise confidence intervals based on the t_{27} distribution.

Our conclusion is that K shows an unambiguous dip (suggesting repulsion or ordered pattern) in the range 15–35 microns and a 'recovery' beyond 35 microns. This combination suggests an ordered pattern; however, it is not clear how much of the dip can be attributed solely to the absence of overlap between osteocyte lacunae (lacunae were roughly ellipsoidal and typically $10 \times 5 \times 5$ microns across, mostly aligned with the main axis in the horizontal plane).

5.4 G function

Estimators $\widehat{G}_1, \widehat{G}_3$ were computed for each brick. Figure 9 shows a comparison of these for a chosen brick, showing the typical non-monotonicity of $\widehat{G}_1$.

However in most cases the individual estimates were absurd (see Figure 10), since both numerator and denominator consisted of only a few points. Recall that a point contributes to the denominator of $\widehat{G}_3$ only when it is closer to its nearest neighbour than to the boundary of the box. In three dimensions this condition becomes very stringent. In our data 23 of the 40 bricks had no point X_k satisfying the condition. No brick had more than three such points. For the same reason the diagnostic scatterplot for ratio regression was nearly meaningless. The behaviour of $\widehat{G}_1$ is slightly better (Figure 11).

Figures 12 and 13 show pooled $\widehat{G}_1$ estimates with pointwise confidence intervals, computed by ratio regression. There is moderate evidence supporting an ordered pattern (short nearest neighbour distances are relatively few).

The alternative un-corrected G estimates G_B were computed and compared with the corresponding Poisson G_B functions for the same bricks, computed numerically by (5). A Monte Carlo test of the Poisson null hypothesis was conducted on each brick independently. Nineteen simulations of a binomial process (i.e. fixed number of independent uniform points) were generated in each brick and ranked by mean nearest neighbour distance. The number of rejections at the 5% level (one-sided in the direction of larger distances) was 7, 8, 9 and 10 bricks for animals 1 to 4 respectively.

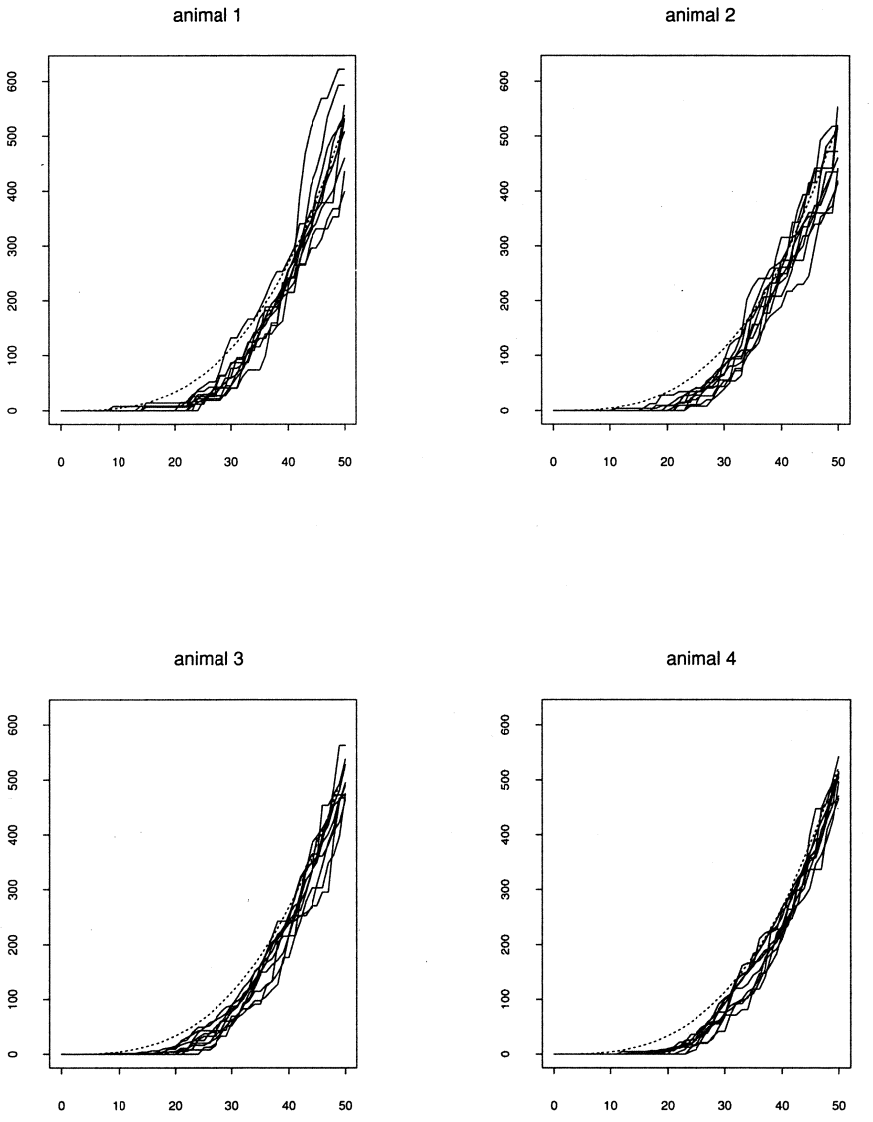

Figure 4: Superimposed K function estimates (isotropic correction) from all bricks for each of the 4 animals.

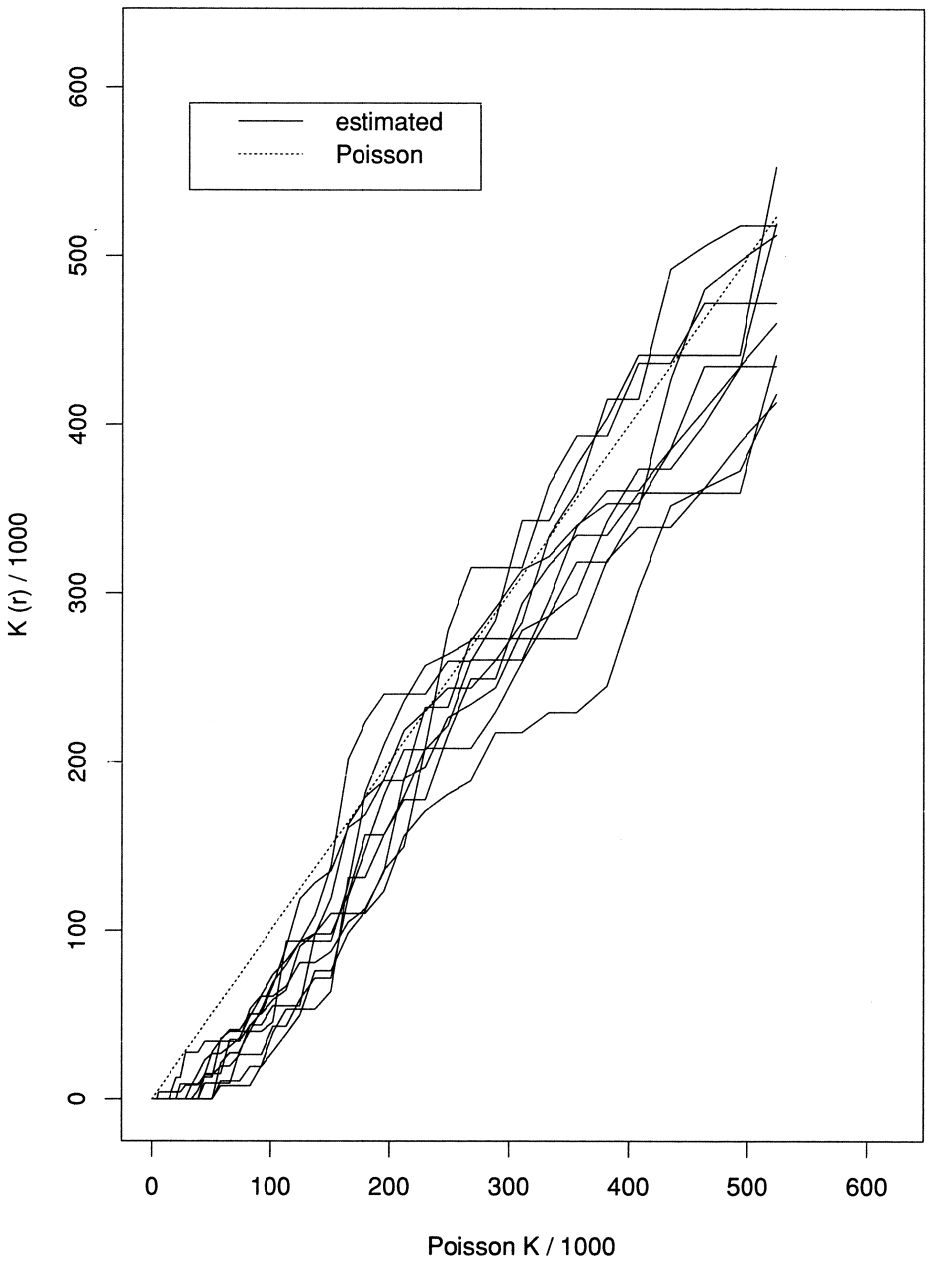

Figure 5: K statistics from each brick in animal 2 plotted Q–Q style.

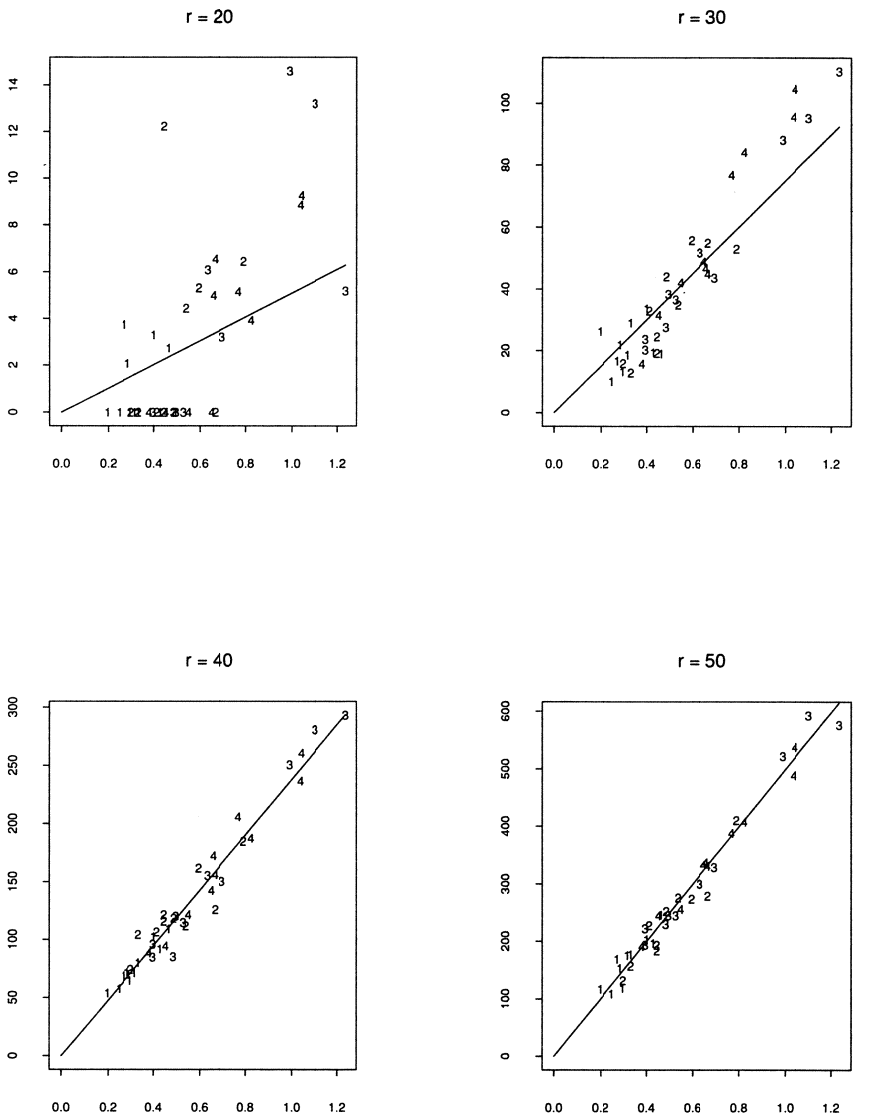

Figure 6: Diagnostic scatter plots of the numerator and denominator of equation (11) for several choices of distance r. Data labelled by animal number.

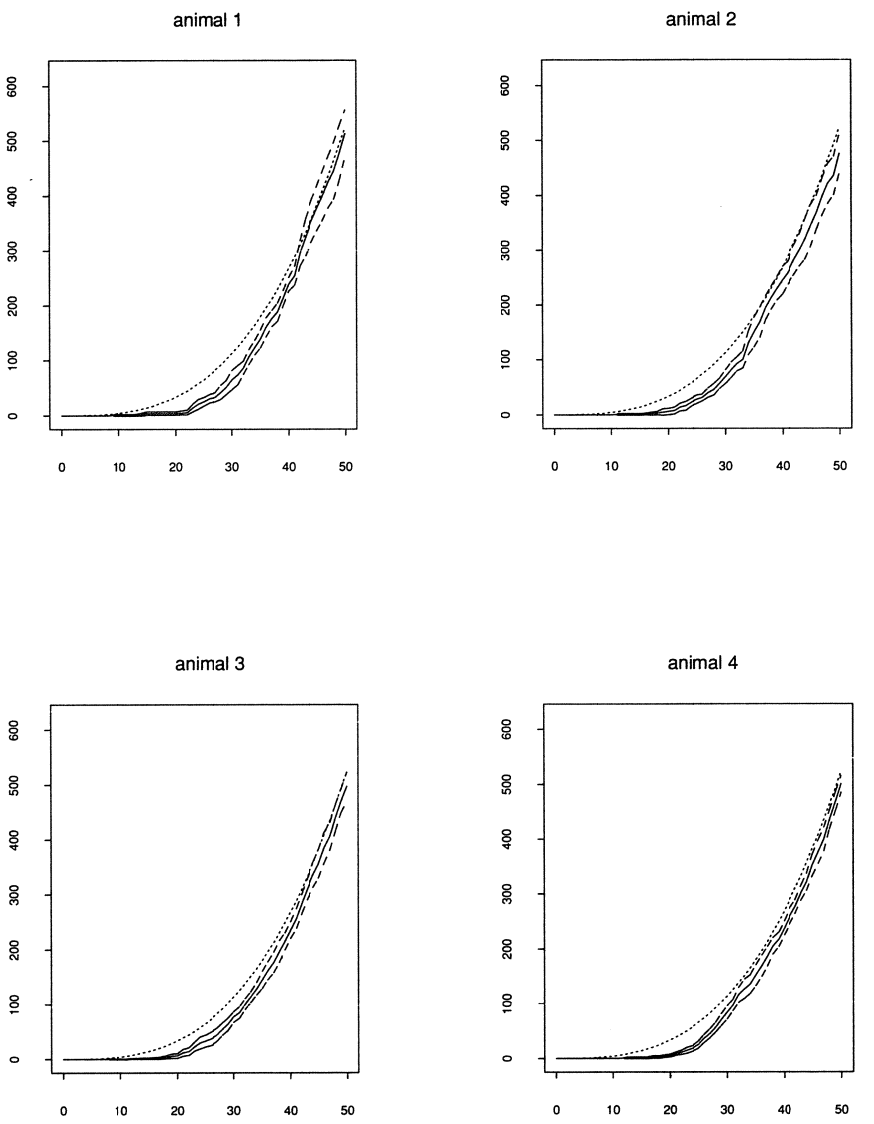

Figure 7: K statistics pooled across bricks within each animal using the ratio regression approach of section 3.

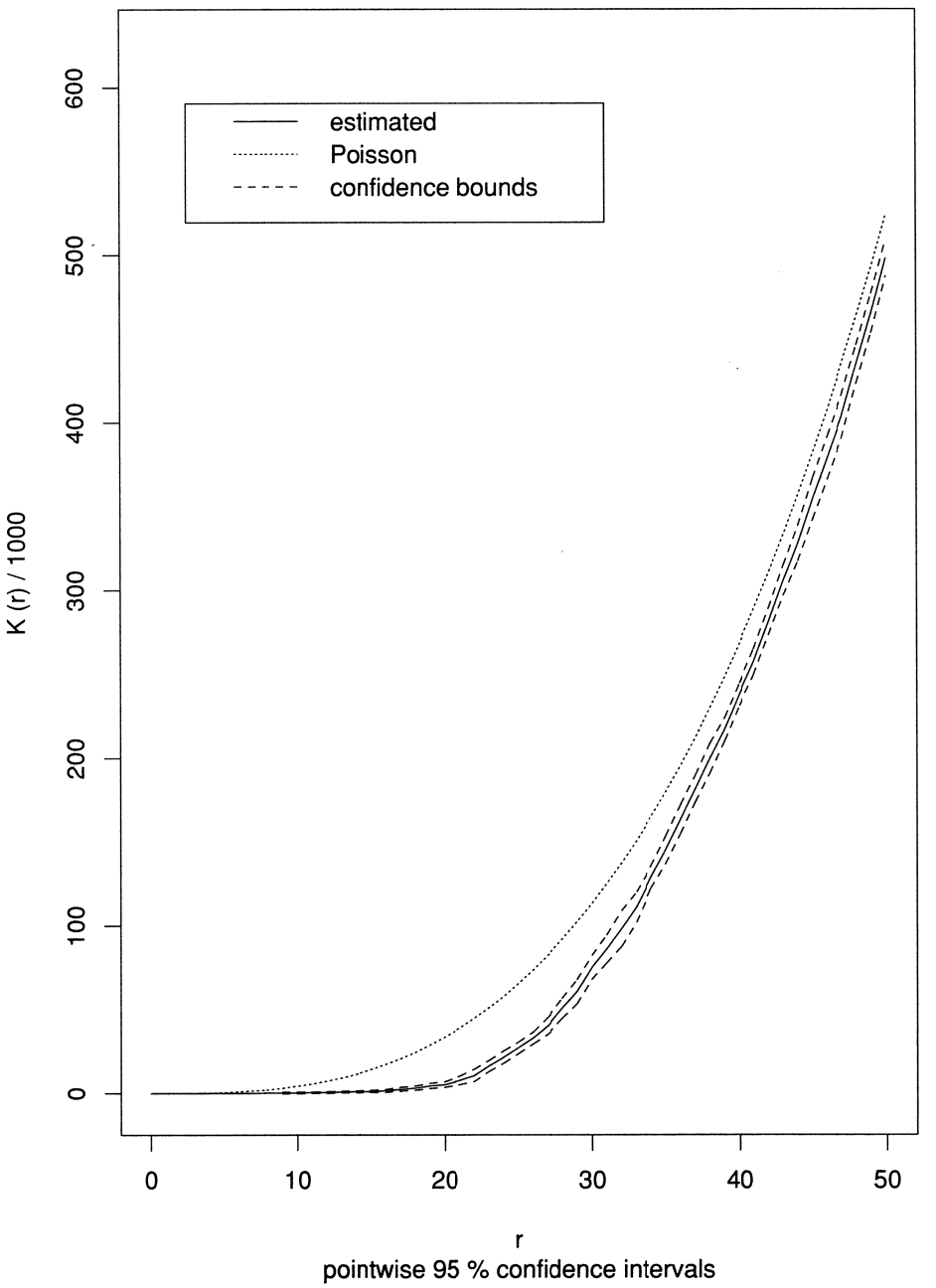

Figure 8: Grand K statistic pooled across all bricks in animals 2,3 and 4, using the E-M approach of section 4. Pointwise confidence intervals based on the t distribution with 27 d.f.

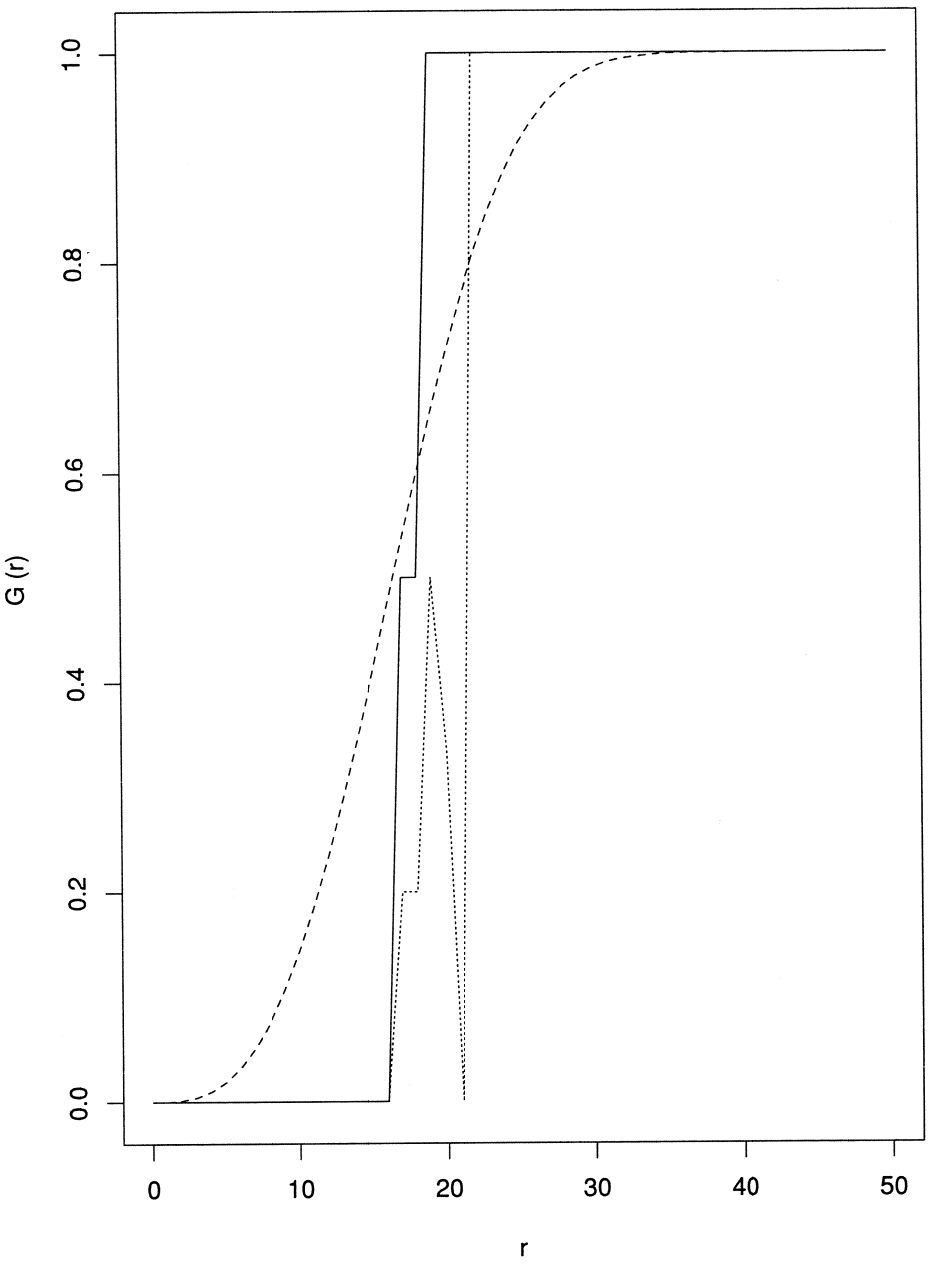

Figure 9: Comparison of G estimates for brick 1 of animal 4, using minus sampling correction (dotted lines) and Hanisch's G_3 (solid lines).

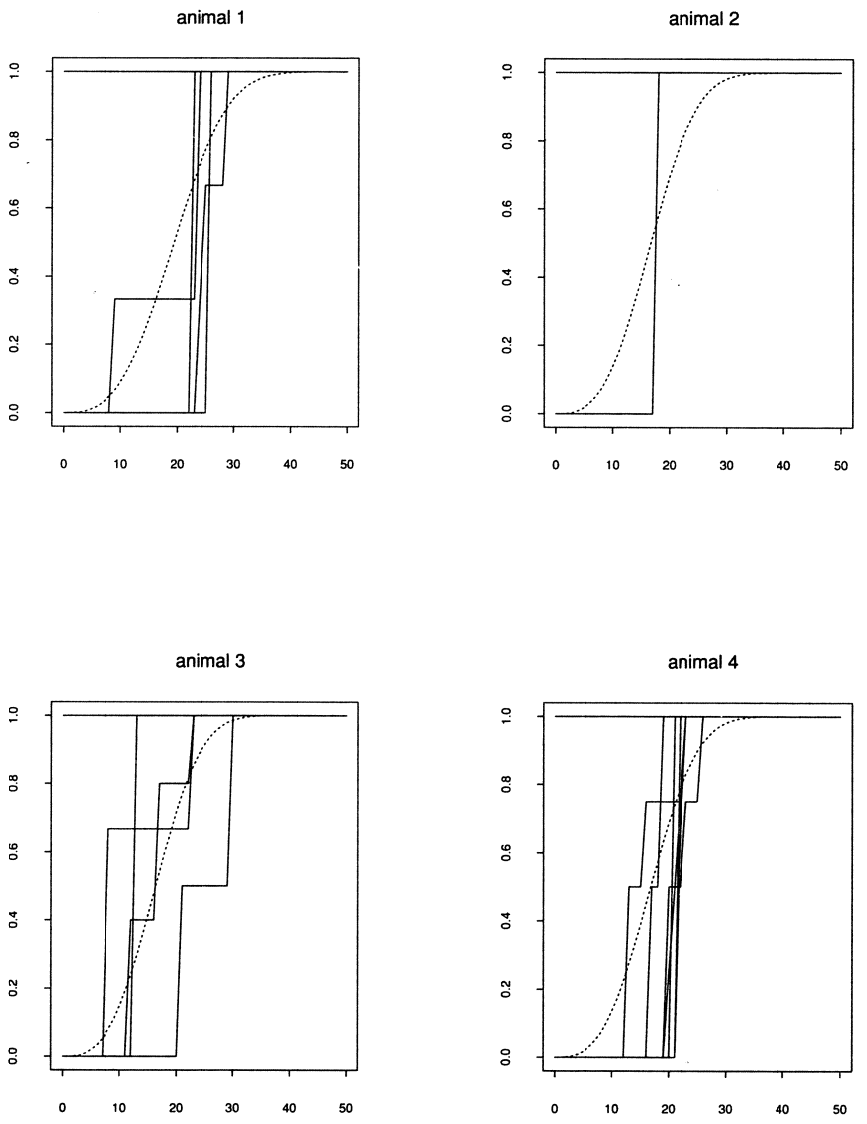

Figure 10: Superimposed plots of G_3 statistics from each brick.

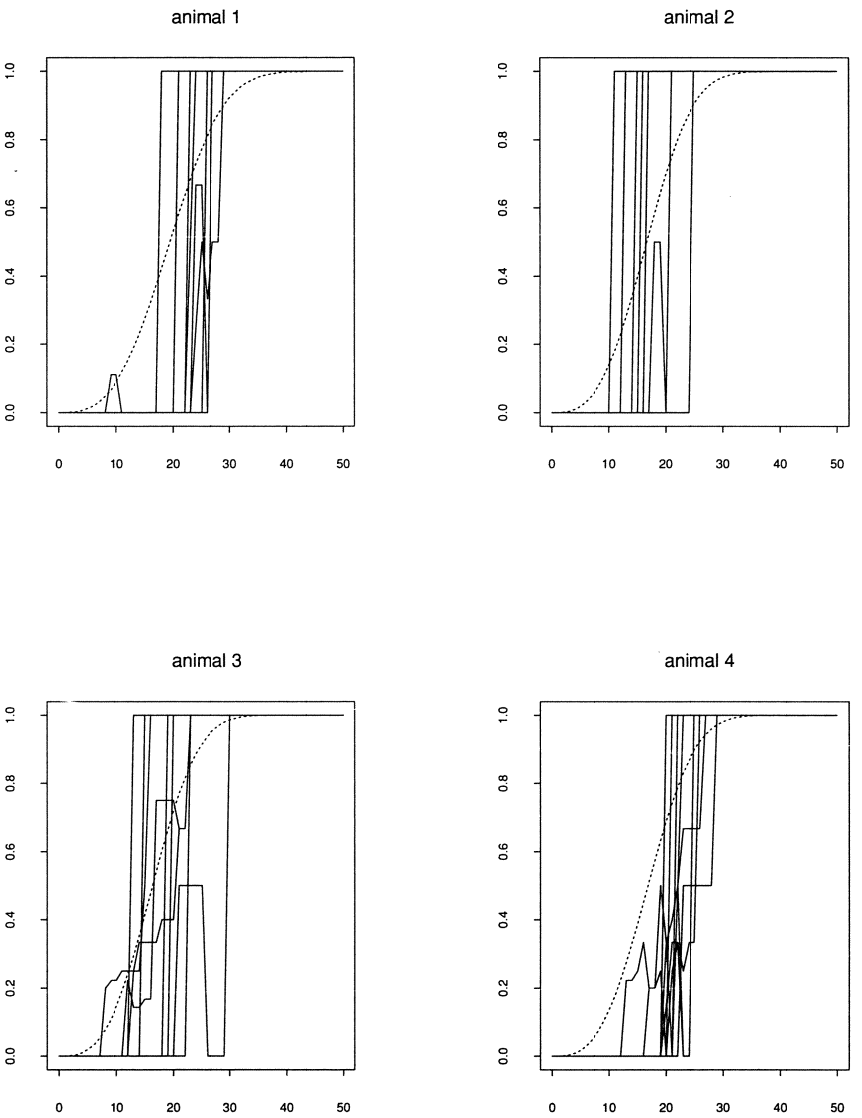

Figure 11: Superimposed plots of G statistics (minus correction) from each brick.

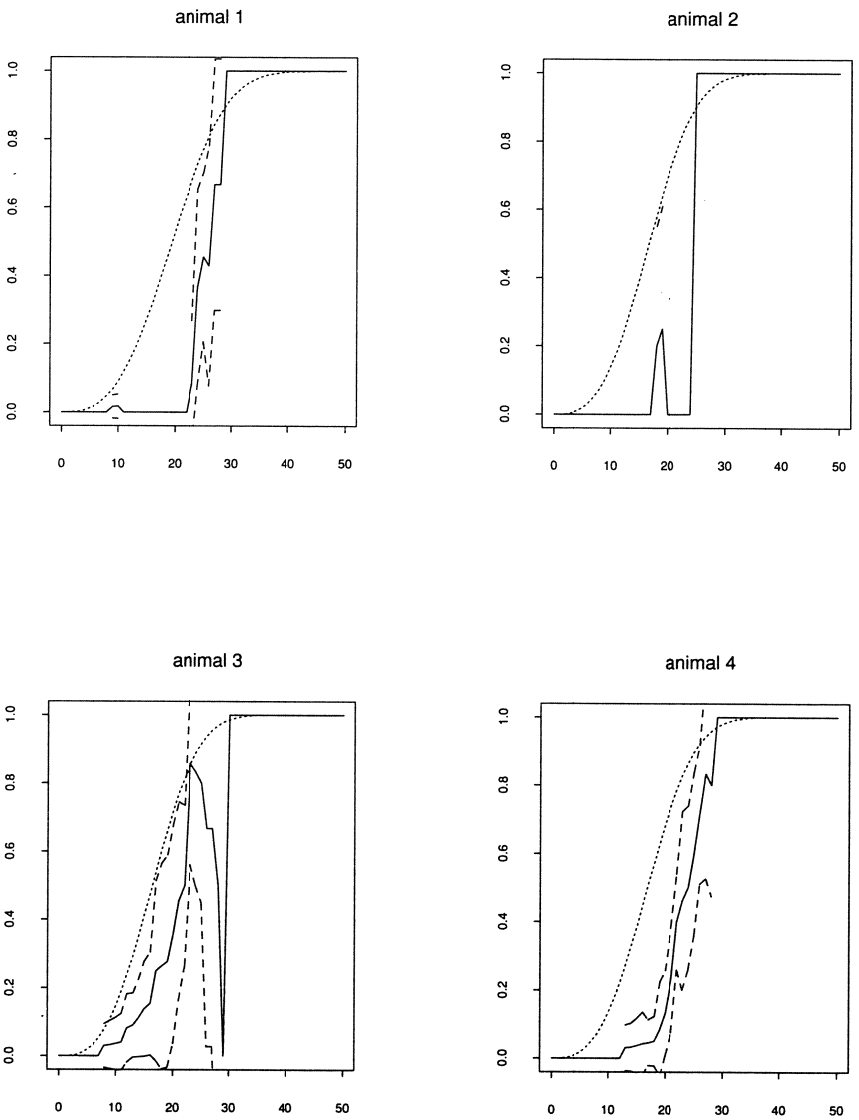

Figure 12: G statistics (minus sampling correction) pooled across bricks within each animal, using the ratio regression approach of section 3.

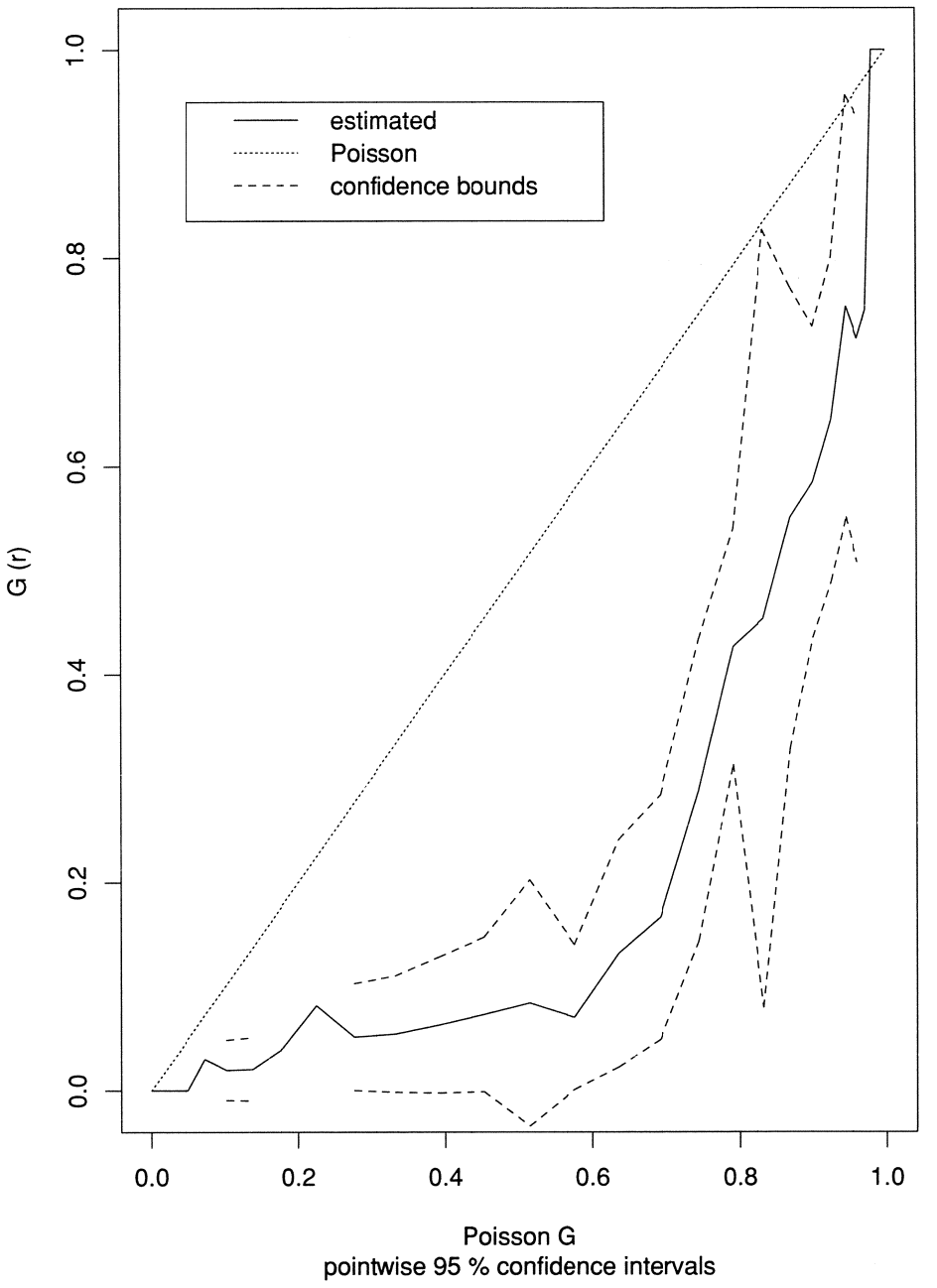

Figure 13: Grand G statistic (minus sampling correction) pooled across animals 2, 3 and 4, using the E-M approach of section 4. Pointwise t_{27} confidence intervals.

5.5 F function

F was estimated by minus sampling (3). We used the discrete distance transform algorithm of Borgefors (1984, 1986) with step distances of 48, 58 and 71, which form a good rational approximation to the proportions $1, \sqrt{2}, \sqrt{3}$. The grid unit or 'voxel' size was 1 micron. The distance $r(x)$ from each x to the boundary of B was also computed and the estimate of F was obtained as the cumulative distribution of the distance transform values $d(x)$ for those voxels satisfying $d(x) \leq r(x)$.

To compute the theoretical Poisson F we determined the volume of the sphere of radius r in the discrete distance function, by running the Borgefors algorithm on a larger grid (large enough to include the entire sphere of radius R equal to the maximum diameter of any brick) and taking a cumulative histogram of the result restricted to the range 0 to R.

Figure 14 shows superimposed F estimates for all bricks in each animal; Figure 15 shows the pooled estimates for each animal, and Figure 16 the population estimate pooled from animals 2, 3 and 4. The Poisson curve lies everywhere outside or on the boundary of the pointwise confidence intervals for these estimates. The plots thus identify a relative shortage of larger empty spaces, again indicative of an ordered pattern.

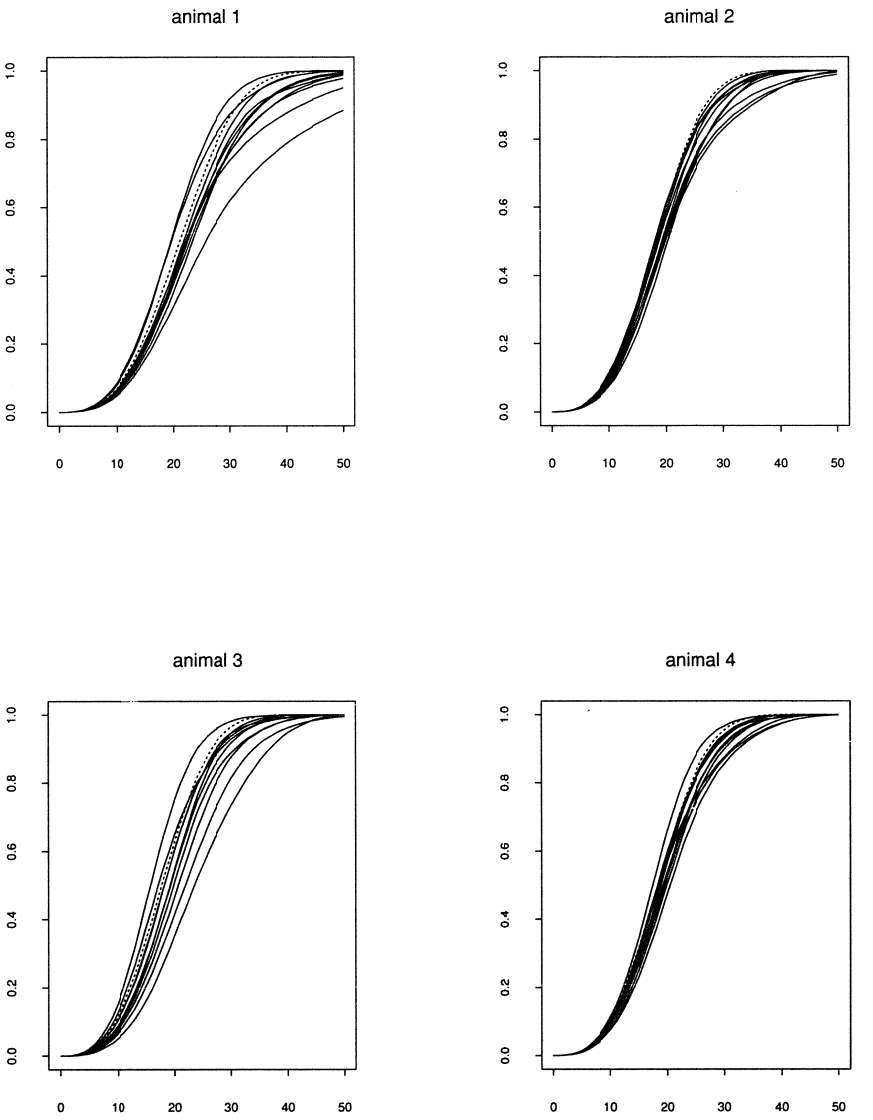

Figure 14: F statistics (digital distance transform, minus correction) for each brick.

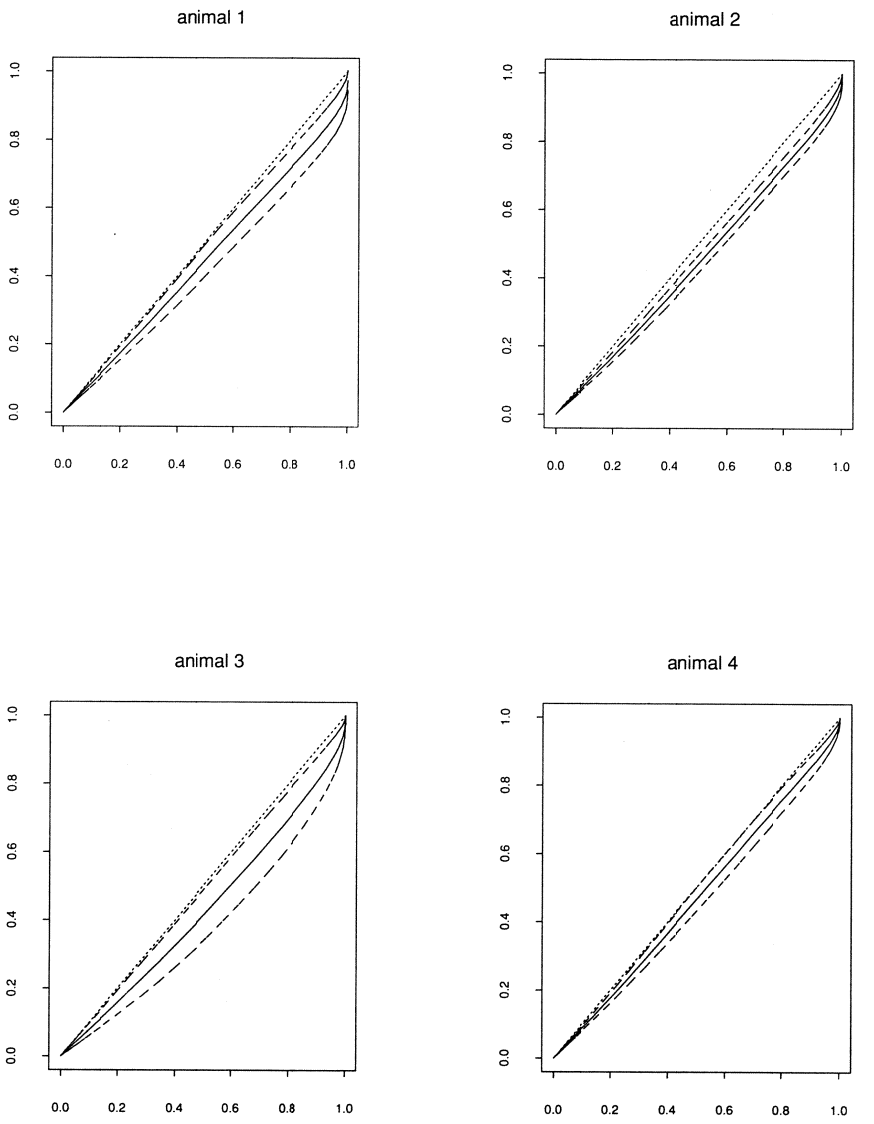

Figure 15: F statistics pooled across bricks using ratio regression (section 3).

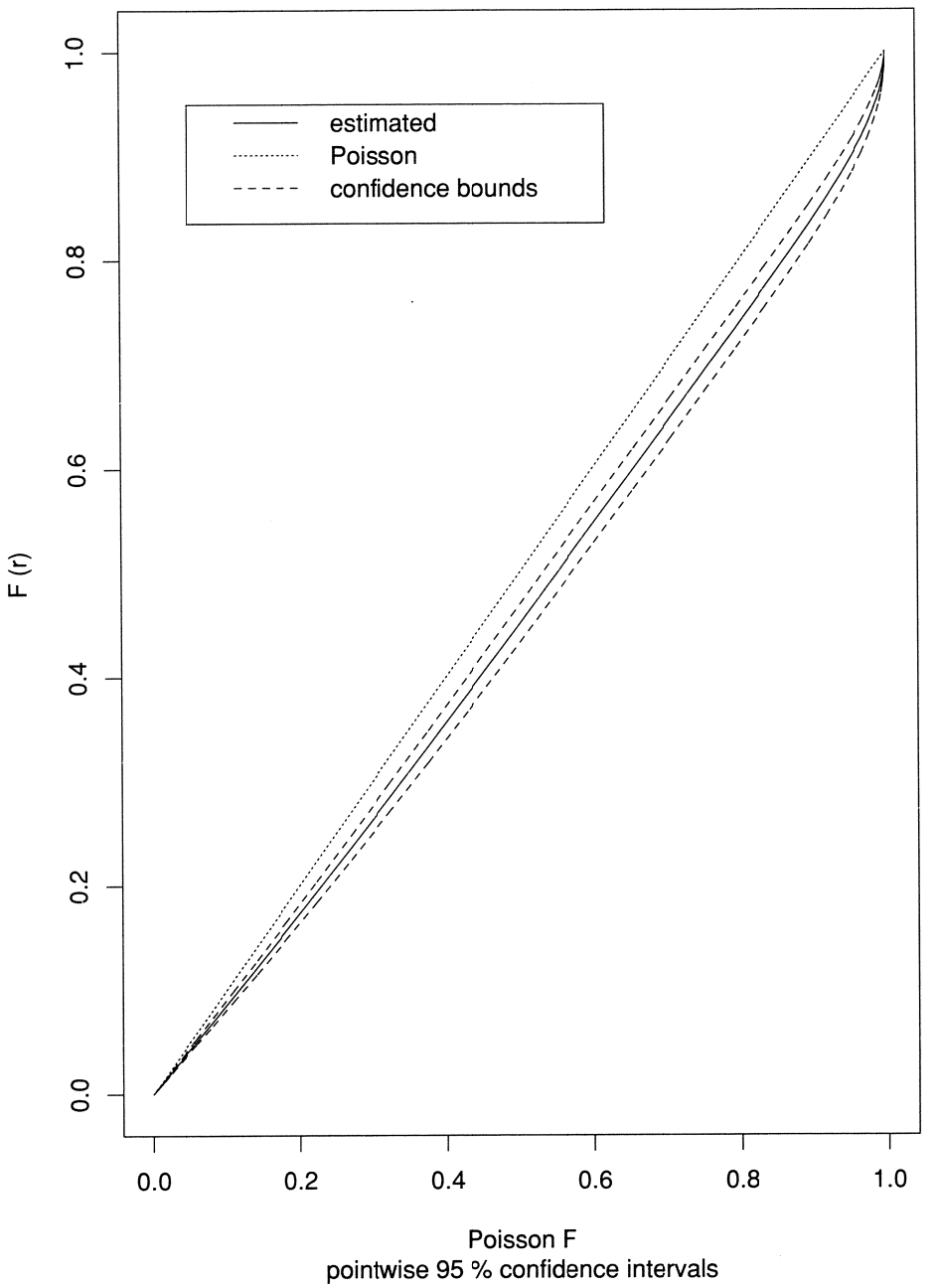

Figure 16: Grand F estimate pooled across animals 2,3 and 4 using E-M technique (section 4).

6 Conclusions

In this paper we adapted standard estimators for two-dimensional F, G, K to three dimensions. The techniques were successful for K and F, but estimation of G is severely hindered by edge effects and should be studied further. It seems to us that the use of kernel smoothing techniques for G (e.g. König et al, 1991) only serves to mask this problem.

The new aspect of replication has been attacked by recognising that the standard estimators are actually ratios of unbiased consistent estimators. Variance arguments suggest the best pooled estimate is the ratio of mean numerator to mean denominator; this seems to be a workable approximation, but for edge effects (for large r) and discrete data effects (for small r). The ratio regression idea also provides standard errors for the pooled estimates. This is new in spatial statistics, since most previous applications have produced confidence bands around the Poisson theoretical curve rather than confidence intervals around the empirical curve.

A rudimentary analysis of variance has also been developed. Its validity is harder to assess from the data studied here, although we did manage to detect an unexpected outlier in the animal population.

Monte Carlo tests of the Poisson null hypothesis were generally rejected, more emphatically when based on F than on G. This accords with the paucity of data in the numerator and denominator of (7),(8). In two dimensions Diggle (1983) found to the contrary that nearest neighbour distances are more powerful than point to nearest event distances against regular alternatives.

There was widespread agreement between animals 2–4 in the K and F functions. All three statistics F, G, K suggested an ordered or regular spatial pattern at a scale of 15–35 microns.

The biological interpretation is uncertain, because this regularity is partly attributable to the physical size of the lacunae (say 5–10 microns across). A similar situation was encountered with the two-dimensional biological cell data discussed by Ripley (1977) and Diggle (1983, p.2). For a biologically conclusive analysis one would need to collect three-dimensional images of entire sampling volumes, and fit a random set model.

Note that it is not always clear how to interpret the *population* mean of a spatial statistic. The population mean of $K(r), F(r), G(r)$ is well-defined, but since the values of F, G for a Poisson process depend on λ, there is no natural benchmark for the population means of $F(r)$ and $G(r)$ unless λ is constant across the population. On the other hand, interpretation of the population mean $K(r)$ is straightforward.

The next step in analysis of the present data could be to model the process by an inhibitive or regular model such as a Markov point process in the standard way (e.g. Ripley, 1988).

Acknowledgements

We thank Peter Diggle for comments and pre-publication copies of his work, and L. Barendregt, L. M. Cruz Orive, R. D. Gill and M. N. M. van Lieshout for helpful comments. Financial support from Nimbus Records Ltd for the Quantitative 3-D Microscopy Research Group, University of Liverpool, is gratefully acknowledged.

References

[1] A J Baddeley. A limit theorem for statistics of spatial data. *Advances in Applied Probability*, 12:447–461, 1980.

[2] A J Baddeley, C V Howard, A Boyde, and S Reid. Three-dimensional analysis of the spatial distribution of particles using the tandem-scanning reflected light microscope. *Acta Stereologica*, 6 (supplement II):87–100, 1987.

[3] A. J. Baddeley and B. W. Silverman. A cautionary example on the use of second-order methods for analyzing point patterns. *Biometrics*, 40:1089–1093, 1984.

[4] J G Bjaalie and P J Diggle. Statistical analysis of corticopontine neuron distribution in visual areas 17,18 and 19 of the cat. *Journal of Comparative Neurology*, 295:15–32, 1990.

[5] G Borgefors. Distance transformations in arbitrary dimensions. *Computer Vision, Graphics and Image Processing*, 27:321–345, 1984.

[6] G Borgefors. Distance transformations in digital images. *Computer Vision, Graphics and Image Processing*, 34:344–371, 1986.

[7] H. Braendgaard and H. J. G. Gundersen. The impact of recent stereological advances on quantitative studies of the nervous system. *J. Neuroscience Methods*, 18:39–78, 1986.

[8] W. G. Cochran. *Sampling Techniques.* John Wiley and Sons, 3rd edition, 1977.

[9] D. R. Cox and V. Isham. *Point processes.* Chapman and Hall, London, 1980.

[10] L. M. Cruz-Orive. Best linear unbiased estimators for stereology. *Biometrics*, 36:595–605, 1980.

[11] P. J. Diggle. *Statistical analysis of spatial point patterns.* John Wiley and Sons, 1983.

[12] P J Diggle and R J Gratton. Monte Carlo methods of inference for implicit statistical models. *Journal of the Royal Statistical Society, Series B*, 46:193–227, 1984.

[13] P J Diggle, N Lange, and F M Benes. Analysis of variance for replicated spatial point patterns in clinical neuroanatomy. *Journal of the American Statistical Association*, 86:???, 1991.

[14] P J Diggle and B Matérn. On sampling designs for the estimation of point-event nearest neighbour distributions. *Scandinavian Journal of Statistics*, 7:80–84, 1981.

[15] I.S. Gradshteyn and I. M. Ryzhik. *Table of Integrals, Series and Products.* Academic Press, 1980.

[16] Peter Hall. *An introduction to the theory of coverage processes.* John Wiley and Sons, New York, 1988.

[17] K H Hanisch. Some remarks on estimators of the distribution function of nearest neighbour distance in stationary spatial point patterns. *Mathematische Operationsforschung und Statistik, series Statistics*, 15:409–412, 1984.

[18] C V Howard, S Reid, A J Baddeley, and A Boyde. Unbiased estimation of particle density in the tandem-scanning reflected light microscope. *Journal of Microscopy*, 138:203–212, 1985.

[19] E. Jolivet. Central limit theorem and convergence of empirical processes for stationary point processes. In P. Bastfai and J. Tomko, editors, *Point processes and queueing problems*, pages 117–161. North-Holland, Amsterdam, 1980.

[20] D. König, S. Carvajal-Gonzalez, A. M. Downs, J. Vassy, and J. P. Rigaut. Modelling and analysis of 3-d arrangements of particles by point processes with examples of application to biological data obtained by confocal scanning light microscopy. *Journal of Microscopy*, 161:405–433, 1991.

[21] H W Lotwick. PhD thesis, University of Bath, 1981.

[22] R E Miles. On the elimination of edge effects in planar sampling. In E F Harding and D G Kendall, editors, *Stochastic Geometry*, pages 228–247. John Wiley and Sons, 1974.

[23] B. D. Ripley. On tests of randomness for spatial point patterns. *Journal of the Royal Statistical Society, Series B*, 41:368–374, 1979.

[24] B. D. Ripley. *Spatial Statistics.* John Wiley and Sons, 1981.

[25] B D Ripley. *Statistical analysis of spatial processes.* John Wiley and Sons, 1988.

[26] A. Rosenfeld and J. L. Pfalz. Distance functions on digital pictures. *Pattern Recognition*, 1:33–61, 1968.

[27] D Stoyan, W S Kendall, and J Mecke. *Stochastic Geometry and its Applications.* John Wiley and Sons, Chichester, 1987.

[28] T Wilson, editor. *Confocal Microscopy.* Academic Press, London, 1990.

Appendix. Sphere volume and surface area

The purpose of this Appendix is to derive expressions for the volume and surface area of the intersection between a three-dimensional rectangular box

$$B = \{\mathbf{x} \in \mathbf{R}^3 : 0 \leq x_i < b_i,\ i = 1,2,3\}$$

with sides $b_i > 0$, and a sphere

$$S(\mathbf{x}, r) = \{\mathbf{y} \in \mathbf{R}^3 : ||\mathbf{y} - \mathbf{x}|| \leq r\}$$

with centre $\mathbf{x} \in B$ and radius $r > 0$. The results are (26), (27), (32) and (33) for volume, and (34), (36) for area.

Thus the aim is to compute

$$\begin{aligned} V(\mathbf{x}, r) &= \mathcal{L}^3(B \cap S(\mathbf{x}, r)) \\ A(\mathbf{x}, r) &= \mathcal{H}^2(B \cap \partial S(\mathbf{x}, r)) \end{aligned}$$

where $\mathcal{L}^3$ is Lebesgue volume measure and $\mathcal{H}^2$ is 2-dimensional Hausdorff (surface area) measure in $\mathbf{R}^3$. Representing B as an intersection of halfspaces

$$B = H_1(0) \cap H_1(b_1)^c \cap H_2(0) \cap H_2(b_2)^c \cap H_3(0) \cap H_3(b_3)^c$$

where $H_i(t) = \{x \in \mathbf{R}^3 : x_i \geq t\}$, and applying the inclusion/exclusion formula, we get

$$\begin{aligned} \frac{4}{3}\pi r^3 - V(\mathbf{x}, r) &= \sum_{i=1}^{3} [V_1(x_i, r) + V_1(b_i - x_i, r)] \\ &\quad - \sum\sum_{i<j} [V_2(x_i, x_j, r) + V_2(x_i, b_j - x_j, r) \\ &\qquad + V_2(b_i - x_i, x_j, r) + V_2(b_i - x_i, b_j - x_j, r)] \\ &\quad + V_3(x_1, x_2, x_3, r) + V_3(x_1, x_2, b_3 - x_3, r) \\ &\quad + V_3(x_1, b_2 - x_2, x_3, r) + V_3(x_1, b_2 - x_2, b_3 - x_3, r) \\ &\quad + V_3(b_1 - x_1, x_2, x_3, r) + V_3(b_1 - x_1, x_2, b_3 - x_3, r) \\ &\quad + V_3(b_1 - x_1, b_2 - x_2, x_3, r) + V_3(b_1 - x_1, b_2 - x_2, b_3 - x_3, r) \end{aligned} \tag{26}$$

where V_1, V_2, V_3 represent the volumes delimited by 1, 2 or 3 halfspaces:

$$\begin{aligned} V_1(t_1, r) &= \mathcal{L}^3(S(0, r) \cap H_1(t_1)) \\ V_2(t_1, t_2, r) &= \mathcal{L}^3(S(0, r) \cap H_1(t_1) \cap H_2(t_2)) \\ V_3(t_1, t_2, t_3, r) &= \mathcal{L}^3(S(0, r) \cap H_1(t_1) \cap H_2(t_2) \cap H_3(t_3)) \end{aligned}$$

for $t_i \geq 0$. If we define $U(a, b, c) = V_3(a, b, c, 1)$ then by symmetry and scaling properties of volume,

$$\begin{aligned} V_1(t_1, r) &= r^3 V_1(t_1/r, 1) = 4r^3 U(t_1/r, 0, 0) \\ V_2(t_1, t_2, r) &= r^3 V_2(t_1/r, t_2/r, 1) = 2r^3 U(t_1/r, t_2/r, 0) \\ V_3(t_1, t_2, t_3, r) &= r^3 U(t_1/r, t_2/r, t_3/r) \end{aligned} \tag{27}$$

It suffices to find an expression for $U(a, b, c)$ when $a, b, c \geq 0$ and $a^2 + b^2 + c^2 < 1$. Now

$$\begin{aligned} U(a,b,c) &= \int_c^{(1-a^2-b^2)^{1/2}} \int_b^{(1-z^2-a^2)^{1/2}} \int_c^{(1-z^2-y^2)^{1/2}} dxdydz \\ &= \int_c^{(1-a^2-b^2)^{1/2}} \int_b^{(1-z^2-a^2)^{1/2}} \{(1-z^2-y^2)^{1/2} - c\} dydz \end{aligned}$$

Using

$$\int (1-a^2-x^2)^{1/2} dx = \frac{1}{2}x(1-a^2-x^2)^{1/2} + \frac{1}{2}(1-a^2)\sin^{-1}\frac{x}{(1-a^2)^{1/2}}$$

this becomes

$$\begin{aligned} U(a,b,c) &= \frac{1}{2}ab(1-a^2-b^2)^{1/2} + \frac{1}{4}ac(1-a^2-c^2)^{1/2} + \frac{1}{4}bc(1-b^2-c^2)^{1/2} \\ &\quad -\frac{1}{4}a(1-a^2)\left(\frac{\pi}{2} - \sin^{-1}\frac{b}{(1-a^2)^{1/2}} - \sin^{-1}\frac{c}{(1-a^2)^{1/2}}\right) \\ &\quad -\frac{1}{4}b(1-b^2)\left(\frac{\pi}{2} - \sin^{-1}\frac{a}{(1-b^2)^{1/2}} - \sin^{-1}\frac{c}{(1-b^2)^{1/2}}\right) \\ &\quad +\frac{\pi}{4}(1-a^2-b^2)^{1/2} - \frac{\pi}{4}c \\ &\quad -\frac{\pi}{12}(1-a^2-b^2)^{3/2} + \frac{\pi}{12}c^3 \\ &\quad -\frac{1}{2}\int_c^{(1-a^2-b^2)^{1/2}} (1-z^2)\sin^{-1}\frac{a}{(1-z^2)^{1/2}} dz \\ &\quad -\frac{1}{2}\int_c^{(1-a^2-b^2)^{1/2}} (1-z^2)\sin^{-1}\frac{b}{(1-z^2)^{1/2}} dz \end{aligned}$$

Here $\sin^{-1}$ maps $(0,1)$ to $(0,\pi/2)$. The remaining terms are integrated by parts with the help of the following identities:

$$\int_0^t (1-A^2-x^2)^{-1/2} dx = \sin^{-1}\frac{t}{(1-A^2)^{1/2}} \tag{28}$$

$$\int_0^t (1-x^2)^{-1}(1-A^2-x^2)^{-1/2} dx = A^{-1}\tan^{-1}\frac{At}{(1-A^2-t^2)^{1/2}} \tag{29}$$

$$\begin{aligned} \int_0^t x^2(1-A^2-x^2)^{-1/2} dx &= \frac{1}{2}(1-A^2)\sin^{-1}\frac{t}{(1-A^2)^{1/2}} \\ &\quad -\frac{1}{2}t(1-A^2-t^2)^{1/2} \end{aligned} \tag{30}$$

$$\begin{aligned} \int_0^t (1-x^2)^{-1}(1-A^2-x^2)^{1/2} dx &= (1-A^2)^{-1/2}\tan^{-1}\frac{t}{(1-A^2-t^2)^{1/2}} \\ &\quad -A(1-A^2)^{-1/2}\tan^{-1}\frac{At}{(1-A^2-t^2)^{1/2}} \end{aligned} \tag{31}$$

holding for $0 < A < 1$, $0 < t < (1-A^2)^{1/2}$. The last three results were suggested by applying the complex identity $\log(a+ib) = \log(a^2+b^2)^{\frac{1}{2}} + i\tan^{-1}(b/a)$ to Gradshteyn & Ryzhik's (1980) formulae §2.584 (69), §2.584 (8) and §2.583 (33). They can be checked directly.

Collecting terms and applying trigonometric identities between $\sin^{-1}$ and $\tan^{-1}$ we finally have

$$\begin{aligned} U(a,b,c) &= \frac{\pi}{12}\{2-3(a+b+c)+(a^3+b^3+c^3)\} \\ &\quad +W(a,b)+W(b,c)+W(a,c)-abc \end{aligned} \tag{32}$$

where

$$\begin{aligned} W(x,y) &= (\frac{1}{2}x-\frac{1}{6}x^3)\tan^{-1}\frac{y}{(1-x^2-y^2)^{1/2}} \\ &\quad +(\frac{1}{2}y-\frac{1}{6}y^3)\tan^{-1}\frac{x}{(1-y^2-x^2)^{1/2}} \\ &\quad -\frac{1}{3}\tan^{-1}\frac{xy}{(1-x^2-y^2)^{1/2}} \\ &\quad +\frac{1}{3}xy(1-x^2-y^2)^{1/2} \end{aligned} \tag{33}$$

The values of $\tan^{-1}$ computed here lie in $[0,\pi/2)$. As a check we can verify the boundary conditions

$$\begin{aligned} U(0,0,0) &= \frac{\pi}{6} \\ U(a,0,0) &= \frac{\pi}{12}\{2-3a+a^3\} \end{aligned}$$

Thus formulae (26), (27), (32) and (33) specify an algorithm for computing $V(\mathbf{x},r)$.

Turning to the surface area problem, we have a decomposition analogous to (26) with $A(\mathbf{x},r)$ replacing $V(\mathbf{x},r)$, A_1,A_2,A_3 replacing V_1,V_2,V_3 and $4\pi r^2$ replacing $\frac{4}{3}\pi r^3$. Analogous to (27) we have

$$\begin{aligned} A_1(t_1,r) &= 4r^2C(t_1/r,0,0) \\ A_2(t_1,t_2,r) &= 2r^2C(t_1/r,t_2/r,0) \\ A_3(t_1,t_2,t_3,r) &= r^2C(t_1/r,t_2/r,t_3/r) \end{aligned} \tag{34}$$

To compute $C(a,b,c)$ for $a,b,c>0$, $a^2+b^2+c^2<1$, parametrise the unit sphere $S(\mathbf{0},1)$ by angular coordinates θ and ϕ defined by

$$u:[0,2\pi)\times(-\frac{\pi}{2},\ \frac{\pi}{2})\to S(\mathbf{0},1)$$

$$u(\theta,\phi)=(\cos\theta\cos\phi,\sin\theta\cos\phi,\sin\phi),$$

i.e. θ represents "longitude" and ϕ is "latitude". The representation of area measure is now

$$u_\sharp dS=\cos\phi\ d\theta\wedge d\phi.$$

Let $T=S(\mathbf{0},1)\cap H_1(a)\cap H_2(b)\cap H_3(c)$ where $a,b,c>0$. Thus $C(a,b,c)=\mathcal{H}^2(T)$ and

$$\begin{aligned} u^{-1}(T) &= \{(\theta,\phi):\cos\theta\cos\phi\geq a,\ \sin\theta\cos\phi\geq b,\ \sin\phi\geq c\} \\ &= \{(\theta,\phi):\sin^{-1}\frac{b}{\sqrt{1-c^2}}\leq\theta\leq\cos^{-1}\frac{a}{\sqrt{1-c^2}}, \\ &\qquad \sin^{-1}c\leq\phi\leq\cos^{-1}(\max(\frac{a}{\cos\theta},\ \frac{b}{\sin\theta}))\} \end{aligned}$$

where henceforth $0 < \theta,\ \phi < \frac{\pi}{2}$. We have

$$\begin{aligned}
C(a,b,c) &= \mathcal{H}^2(T) \\
&= \int_{\sin^{-1}\frac{b}{\sqrt{1-c^2}}}^{\cos^{-1}\frac{a}{\sqrt{1-c^2}}} \int_{\sin^{-1} c}^{\cos^{-1}(\max(\frac{a}{\cos\theta},\frac{b}{\sin\theta}))} \cos\phi \; d\phi d\theta \\
&= \int_{\sin^{-1}\frac{b}{\sqrt{1-c^2}}}^{\tan^{-1}\frac{b}{a}} \int_{\sin^{-1} c}^{\cos^{-1}(\frac{b}{\sin\theta})} \cos\phi \; d\phi d\theta \\
&\quad + \int_{\tan^{-1}\frac{b}{a}}^{\cos^{-1}\frac{a}{\sqrt{1-c^2}}} \int_{\sin^{-1} c}^{\cos^{-1}(\frac{a}{\cos\theta})} \cos\phi \; d\phi d\theta \\
&= \int_{sin^{-1}\frac{b}{\sqrt{1-c^2}}}^{\tan^{-1}\frac{b}{a}} \sqrt{1-\frac{b^2}{\sin^2\theta}}\, d\theta + \int_{\tan^{-1}\frac{b}{a}}^{\cos^{-1}\frac{a}{\sqrt{1-c^2}}} \sqrt{1-\frac{a^2}{\cos^2\theta}}\, d\theta \\
&\quad + c(\sin^{-1}\frac{b}{\sqrt{1-c^2}} - \cos^{-1}\frac{a}{\sqrt{1-c^2}}) \\
&= I(\cos^{-1}\frac{a}{\sqrt{1-c^2}}, a) - I(\tan^{-1}\frac{b}{a}, a) \\
&\quad + I(\cos^{-1}\frac{b}{\sqrt{1-c^2}}, b) - I(\tan^{-1}\frac{a}{b}, b) \\
&\quad + c[\sin^{-1}\frac{b}{\sqrt{1-c^2}} - \cos^{-1}\frac{a}{\sqrt{1-c^2}}]
\end{aligned} \tag{35}$$

where the range of $\tan^{-1}$ is $(-\frac{\pi}{2},\ \frac{\pi}{2})$ and

$$I(t,A) = \int_0^{\sin t} \frac{\sqrt{1-A^2-x^2}}{1-x^2} dx$$

for $0 < A < 1$, $0 < t < \sin^{-1}(1-A^2)^{\frac{1}{2}}$. Substituting (31) we finally obtain

$$\begin{aligned}
C(a,b,c) &= \tan^{-1}\left[\frac{(1-a^2-c^2)^{\frac{1}{2}}}{ac}\right] + \tan^{-1}\left[\frac{(1-b^2-c^2)^{\frac{1}{2}}}{bc}\right] \\
&\quad + \tan^{-1}\left[\frac{(1-a^2-b^2)^{\frac{1}{2}}}{ab}\right] - a\tan^{-1}\left[\frac{(1-a^2-c^2)^{\frac{1}{2}}}{c}\right] \\
&\quad + a\tan^{-1}\left[\frac{b}{(1-a^2-b^2)^{\frac{1}{2}}}\right] - b\tan^{-1}\left[\frac{(1-b^2-c^2)^{\frac{1}{2}}}{c}\right] \\
&\quad + b\tan^{-1}\left[\frac{a}{(1-a^2-b^2)^{\frac{1}{2}}}\right] - c\tan^{-1}\left[\frac{(1-a^2-c^2)^{\frac{1}{2}}}{a}\right] \\
&\quad + c\tan^{-1}\left[\frac{b}{(1-b^2-c^2)^{\frac{1}{2}}}\right] - \pi
\end{aligned} \tag{36}$$

when $a^2 + b^2 + c^2 < 1$, and $C(a,b,c) = 0$ otherwise. Here the values of $\tan^{-1}$ lie in $(0, \frac{\pi}{2})$. As a check, one can verify the boundary conditions

$$C(u,0,0) = C(0,u,0) = C(0,0,u) = \frac{\pi}{2}(1-u),$$

$$C\left(\frac{1}{\sqrt{3}}, \frac{1}{\sqrt{3}}, \frac{1}{\sqrt{3}}\right) = 0.$$

Thus (34) and (36) specify an algorithm for computing the surface area $A(\mathbf{x}, r)$ and the edge-effect correction factor

$$w(\mathbf{x}, r) = \frac{A(\mathbf{x}, r)}{4\pi r^2}.$$

Acknowledgement

We thank Dr C.C. Taylor (University of Leeds) for the suggestion leading to (29 – 31).